International Atomic Energy Agency

INDC(CCP)-373
Distr.: L

INDC INTERNATIONAL NUCLEAR DATA COMMITTEE

SECONDARY NEUTRON SPECTRA FROM SPHERICAL AND HEMISPHERICAL SAMPLES OF STRUCTURAL MATERIALS INDUCED BY 14 MeV NEUTRONS

A.I. Saukov, B.I. Sukhanov and A.M. Ryabinin
All-Union Scientific Research Institute of Technical Physics
Chelyabinsk, Russia

(Translated from a Russian original published in
Yadernye Konstanty 4/1991, pages 3-25)

Translated by the IAEA

July 1994

Reproduced by the IAEA in Austria
July 1994

INDC(CCP)-373
Distr.: L

94-10589 (C)
Translated from Russian

UDC 539.171.4

SECONDARY NEUTRON SPECTRA FROM SPHERICAL AND HEMISPHERICAL SAMPLES OF STRUCTURAL MATERIALS INDUCED BY 14 MeV NEUTRONS

A.I. Saukov, B.I. Sukhanov and A.M. Ryabinin
All-Union Scientific Research Institute of Technical Physics
Chelyabinsk

ABSTRACT

The authors present the results of time-of-flight measurements of secondary neutron spectra in the 0.4-14 MeV energy range for spherical and hemispherical samples of structural materials and the elements Mg, Al, Fe, Ti, Ni, Cu, Zr, Mo, CF_2, Pb, ^{238}U, H_2O, D_2O, Be, C and CH_2 induced by 14 MeV neutrons. The dependence of the relative neutron detector efficiency on energy is given. The final results are presented in the form of normalized instrumental spectra and also in the form of neutron yield tables in 13 energy ranges from 0.4 to 14 MeV. The results may be used for checking and correcting existing data for the materials and elements investigated.

In recent years, interest in so-called integral experiments designed to check the whole set of neutron constants for a particular element has grown [1]. We therefore carried out a series of experiments to measure the neutron spectra emitted by spherical and hemispherical samples of various structural elements and materials under the effect of 14 MeV neutrons. We studied the following: Mg, Al, Fe, Ti, Ni, Cu, Zr, Mo, CF_2, Pb, ^{238}U, H_2O, D_2O, Be, C and CH_2. We find the results obtained using hemispherical samples (inverted hemispheres) particularly interesting since they can be used to check the large-angle elastic and inelastic

neutron scattering constants which are difficult to measure in small samples and for which the measurement accuracy is usually low.

The measurements were performed using the time-of-flight method with a path length of 8.5 m, a detector with a 70 x 70 mm stilbene crystal and an FEhU-110 photomultiplier with n-γ separation to reduce the gamma-ray background. The neutron registration threshold was 0.15 MeV. The pulsed neutron generator had the following parameters:

Neutron pulse length - 15 ns;

Pulse repetition rate - 500 kHz;

Mean neutron yield - $3 \cdot 10^8$ n/s.

In order to reduce the flux of direct 14 MeV neutrons and obtain more accurate information on the extent of elastic scattering of 14 MeV neutrons in the samples, a steel bar 30 mm in diameter and 400 mm long was placed between the target and the detector which totally covered the accelerator target (target diameter: 25 mm) and only slightly affected the flux of neutrons scattered in the sample. The sample parameters are given in Table 1 and the geometry of the experiment is shown in Fig. 1.

All the experimental results were normalized to 1000 14 MeV neutrons registered by the detector from the free target minus the shielding rod.

Following many experiments and calculations, a detector efficiency value was adopted which was based on a comparison of the experimental and calculated spectrum for a spherical ^{238}U sample. (The ^{238}U, CH_2 and Pb spectra were calculated using the Monte Carlo method in Refs [2, 3].) The relative detector efficiency value which we adopted is shown in Table 2. In order to establish more accurately the energy dependence of the detector efficiency employed, independent measurements were carried out at 1.48 and 2.64 MeV using annular polyethylene scatterers. The results of these measurements, which are based on the well-

known elastic scattering cross-section for 14 MeV neutrons in hydrogen, agreed with the efficiency value adopted by us to an accuracy of $\pm$ 4%. The high level of agreement between the calculated and experimental spectra for such widely studied materials as polyethylene and lead is further evidence in support of this detector efficiency value. Overall, we estimate that the error level of our detector efficiency value is $\pm$ 5% at most.

In addition, by using the ^{238}U spectrum as the basis for our measurements, we are proof against errors caused by a change in the experiment geometry, shifts in the registration thresholds and replacement and deterioration of the detector crystals. This approach to determining the detector efficiency means that the results obtained by us can be reproduced in other laboratories. If it should transpire that the ^{238}U neutron spectrum which we adopted as our standard differs somewhat from the real spectrum, then the relevant corrections can be introduced using measurements performed on other samples.

The detector efficiency includes scattering of neutrons in the air (for a path length of L = 8.5 m) and scattering in the materials surrounding the detector (crystal packaging, photomultiplier tube, detector housing and shielding. Since all of these effects are, to some extent, resonance-like in nature (particularly scattering in air), the detector efficiency should, strictly speaking, reflect this resonance structure. Since this structure does not exceed 4-5% over the larger portion of the spectrum at our energy resolution, we found it possible to maintain a smooth efficiency curve except in the 920 ns region (neutron energy E_n = 0.44 MeV) where the strong oxygen resonance causes a dip of up to 15% in the efficiency curve.

All the measurement results are given in the form of instrumental spectra $\Delta N/\Delta t$ relative to the time of flight of the neutrons in time intervals of $\Delta t = 10^{-8}$ s. This way of presenting the data has specific advantages by comparison with the traditional energy-

dependent mode of presentation: $\Delta n/\Delta E = f(E_n)$. In normal co-ordinates, the neutron spectrum tends to infinity when the neutron energy tends to zero. Under these conditions, measurement errors increase sharply when the neutron energy approaches the registration threshold. Moreover, at high energies ($E_n > 8$ MeV) the energy resolution capacity of the time-of-flight method decreases sharply, reaching $\pm$ 1.2 MeV at around 14 MeV, whereas the resolution capacity is 0.022 MeV at a neutron energy of 0.5 MeV.

This makes the graph of the neutron spectrum terribly difficult to read in normal co-ordinates, since the larger part of it is taken up by uninformative data with a high error level and the main part of the spectrum is concentrated in an insignificant area on a small scale. By contrast, when the instrumental spectrum is presented as a function of the time of flight, the error levels both as regards the time and the amplitude are distributed practically evenly over the whole area of the graph.

The statistical accuracy of the experiments in the 1-3 MeV region, where the main group of neutrons is concentrated, was at least $\pm$ 2%. We estimate the overall accuracy level in this region to be $\pm$ 5%.

The measurement results are shown in Figs 2-33 and are summarized in Table 3 which presents numerical data that take into account the detector efficiency for discrete energy intervals from 0.4 to 15 MeV. All the data shown in Figs 2-33 and in Table 3 are normalized to 1000 14 MeV neutrons.

Before moving on to a discussion of the results, let us look at Fig. 34 which shows a ^{238}U spectrum after passage of a particle through a layer of Be 2 cm thick. This spectrum, which is given in relative units, is used mainly for energy calibration of the time-of-flight spectrometer. The marked dip at 780 ns (0.62 MeV in energy terms) corresponds to a pronounced resonance in the total cross-section for beryllium. Apart from its main object,

this figure shows how the time resolution of this method is practically independent of the time of flight, since the natural width of the resonance for beryllium was not increased in our measurements.

Integral experiments on spherical samples with 14 MeV neutrons have also been performed in other laboratories. In Ref. [4], measurements are performed for carbon, oxygen, aluminium, titanium and iron. In Ref. [5] the leakage spectra from a water sphere are measured, in Refs [6, 7] the spectra from iron spheres, in Refs [8, 9] the spectra from lead, and in Refs [10, 11] the spectra from uranium-238 and beryllium.

Unfortunately, it is difficult to make direct comparisons between data produced in different laboratories, since the experiments were performed under different conditions with samples of different sizes. Therefore, the results obtained by the various authors may be compared only by performing the relevant calculations using one or another set of nuclear physics constants. Although in each of the above-mentioned papers, to some extent, calculations were performed and a comparison made with experiments in the laboratory in question, no comparison was made with experiments from different laboratories, which means that it is impossible to determine possible errors in experiment and calculation. A partial attempt at a comparison of experimental data from various sources is made in Ref. [3] for ^{238}U, CH_2 and Pb, and it is intended to extend this to other elements and materials.

It should also be noted that the published data has only limited informational value. For example, in Ref. [4], only data for neutrons with an energy of over 2 MeV are given for the leakage spectra from C, O, Al, Fe and Ti, which makes it impossible to check the neutron constants of elements for the main group of inelastic scattering neutrons below 2 MeV. As a rule, data are presented in figures with a logarithmic scale and no numerical data are given, which also hampers comparison of results. It would be desirable for

laboratories to agree on standardized sample dimensions and standardized methods of presenting data, as is the case for standard measurements of reference neutron cross-sections, in order to facilitate accurate intercomparison of both experimental data and the accepted versions of libraries of evaluated data.

REFERENCES

[1] TRYKOV, L. A., Integral Experiments on Ionizing Radiation Transport, Ehnergoizdat, Moscow (1985) [in Russian].

[2] VASIL'EV, A. P., KANDIEV, Ya. Z., KUROPATENKO, Eh. S., "Measurements and Calculations of 14 MeV Neutron Scattering in Spherical Pb Samples", Neutron Physics, Kiev (1987) [in Russian].

[3] VASIL'EV, A. P., LYUTOV, V. D., KANDIEV, Ya. Z., Checking the Neutron Constants for ^{238}U, Be, CH_2 and Pb against the Results of Measurements on Spherical Samples, Report VNIITF [All-Union Scientific Research Institute of Technical Physics] (1989) [in Russian].

[4] HANSEN, L. E., WONG, C., KOMOTO, T., ANDERSON, J. D., Nucl. Sci. Eng. **60** 1 (1976) 27.

[5] STELTS, M. L., ANDERSON, J. D., HANSEN, L. F., PLECHATY, E. F., WONG, C., Nucl. Sci. Eng. **46** 1 (1971) 53.

[6] HANSEN, L. F., ANDERSON, J. D., BROWN, P. S., HOWERTON, R. J., et al., Nucl. Sci. Eng. **51** 3 (1973) 278.

[7] DEVKIN, B. V., ZHURAVLEV, B. V., KOBOZEV, M. G., LYCHAGIN, A. A., et al., Problems of Nuclear Science and Technology, Series: Nuclear Constants, No. 2 (1990) 5 [in Russian].

[8] HANSEN, L. F., et al., NSF 92 (1986) 382.

[9] YANAGI, Y., TAKAHASHI, A., Report A-84-02, Osaka (1984).

[10] WONG, C., et al., Washington Conference on Neutron Cross Sections, Washington (1975) 704.

[11] HANSEN, L. F., et al., NSE 72 (1979) 35.

[12] ANDROSENKO, A. A., et al., Proc. Int. Conf. on Neutron Physics, Kiev (1987) 194 [in Russian].

Table 1

Sample parameters

No.	Sample	Mass of inverted hemisphere, kg	Mass of sphere, kg	Sample dimensions, mm
1	*Mg*	3,260	6,590	200x100
2	*Al*	4,880	9,860	200x100
3	*Fe*	13,330	26,900	198x99
4	*Ti*	7,920	16,170	200x100
5	*Ni*	14,820	29,910	200x100
6	*Cu*	14,750	29,920	197x100
7	*Zr*$^{*)}$	11,710	23,660	200x98
8	*Mo*$^{*)}$	17,810	36,070	200x100
9	$[CF_2]_n$	3,900	7,860	200x100
10	*Pb*	19,250	39,110	200x100
11	^{238}U	33,300	67,800	200x100
12	H_2O	1,780	3,600	200x100
13	D_2O	1,96	3,95	200x100
14	*Be*	6,300	12,670	260x160
15	*C*	2,215	4,550	180x100
16	$[CH_2]_n$	1,620	3,280	200x100

These samples were taken from sheet material and the mean density may therefore be slightly different from normal.

Table 2

Detector efficiency

Time, ns	ϵ, rel.	Time, ns	ϵ, rel.	Time, ns	ϵ, rel.
100	1,0	40	1,47	80	1,71
20	1,0	60	1,50	800	1,73
40	1,0	80	1,52	20	1,75
60	1,0	500	1,54	40	1,76
80	1,0	20	1,55	60	1,73
200	1,02	40	1,56	80	1,65
20	1,04	60	1,56	900	1,56
40	1,08	80	1,57	20	1,50
60	1,12	600	1,58	40	1,50
80	1,17	20	1,59	60	1,52
300	1,22	40	1,61	80	1,55
20	1,26	60	1,64	1000	1,53
40	1,31	80	1,67	20	1,50
60	1,35	700	1,68	40	1,45
80	1,39	20	1,69	60	1,40
400	1,42	40	1,69	80	-
20	1,44	60	1,70	1100	-

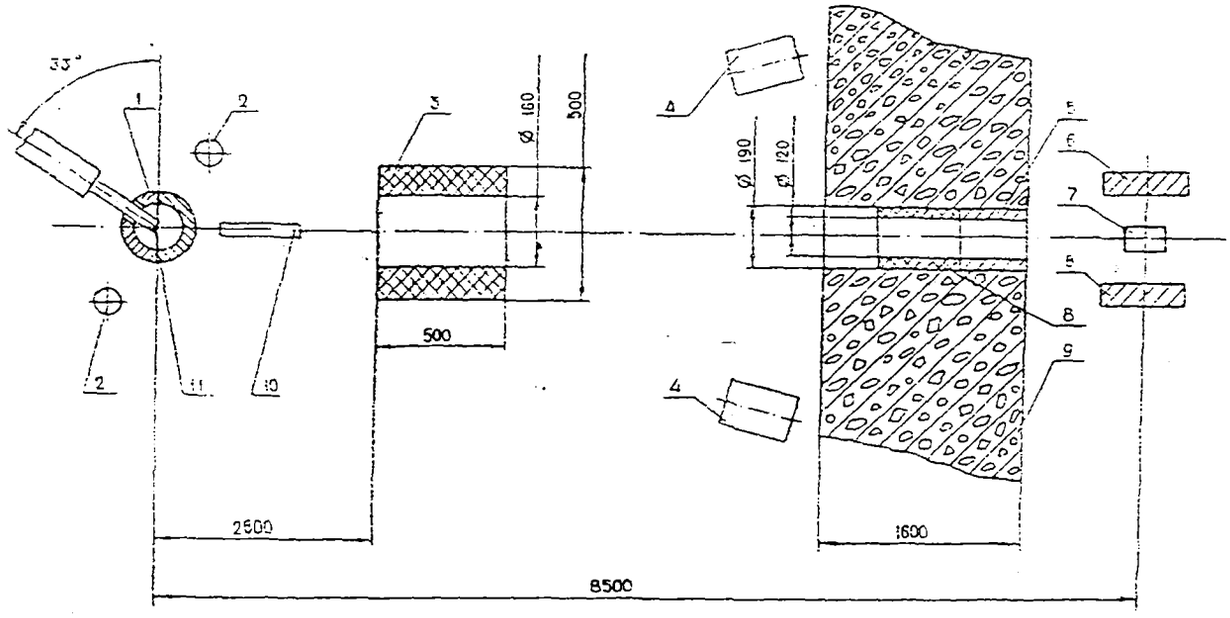

Fig. 1. Geometry of the experiment: 1 - sample to be measured; 2 - pulsed neutron flux monitors; 3 - polyethylene collimator; 4 - all-wave counters; 5 - lead collimator; 6 - lead detector shield; 7 - detector; 8 - polyethylene collimator; 9 - concrete wall; 10 - steel rod; 11 - 14 MeV source.

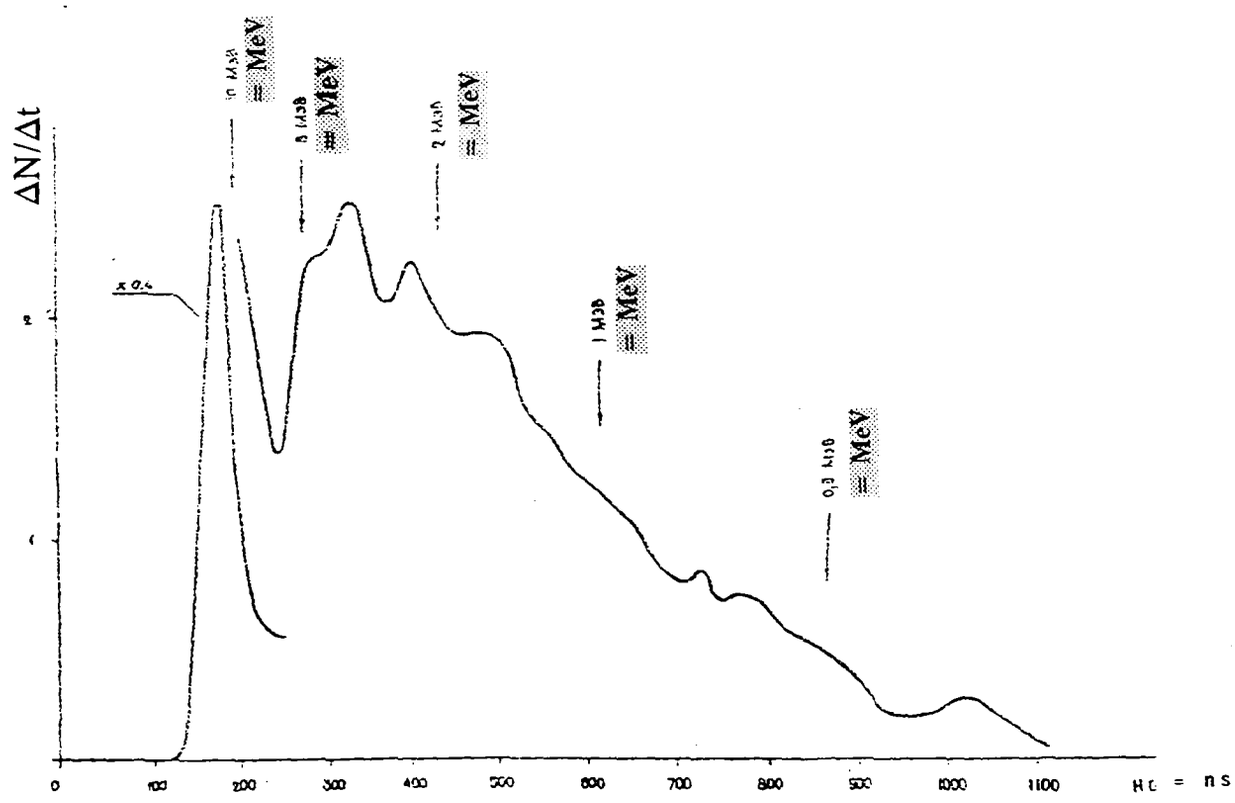

Fig. 2. Normalized instrumental spectrum from a hemispherical magnesium sample.

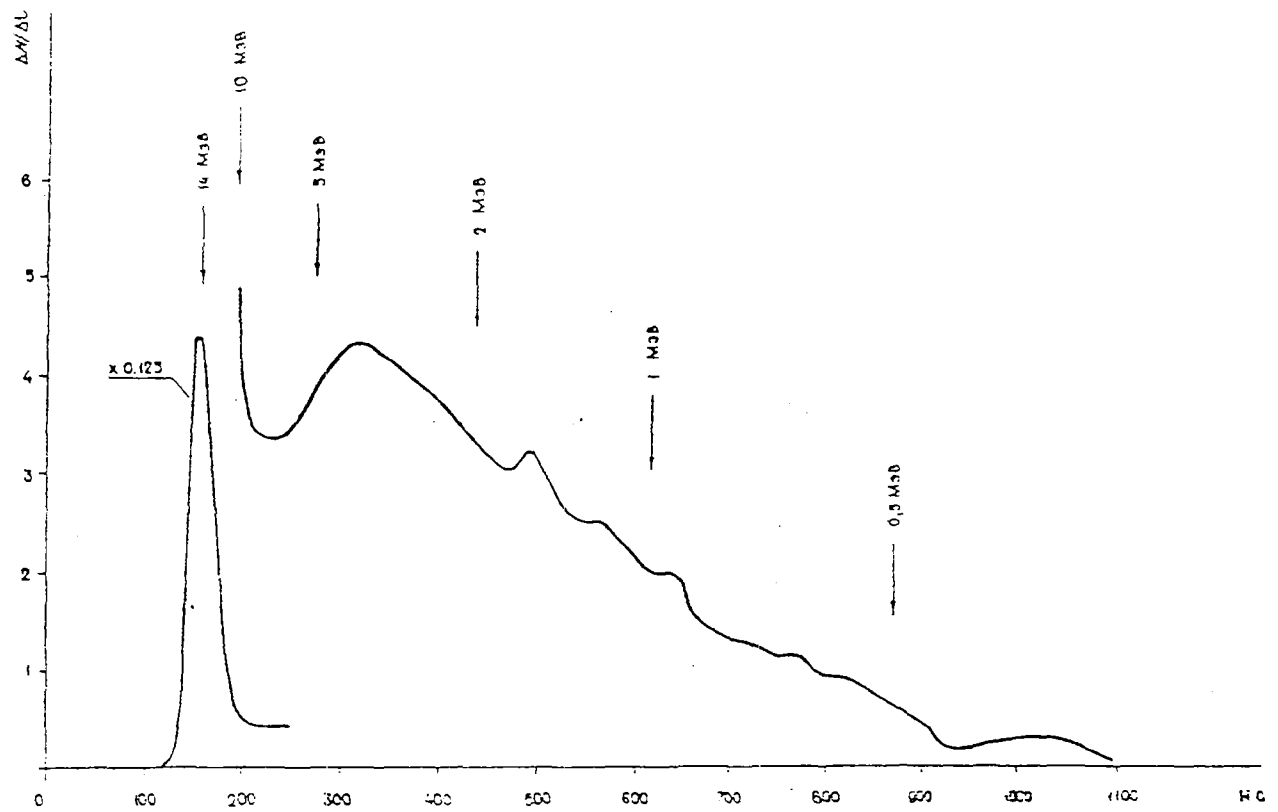

Fig.3. Normalized instrumental spectrum from a spherical magnesium sample.

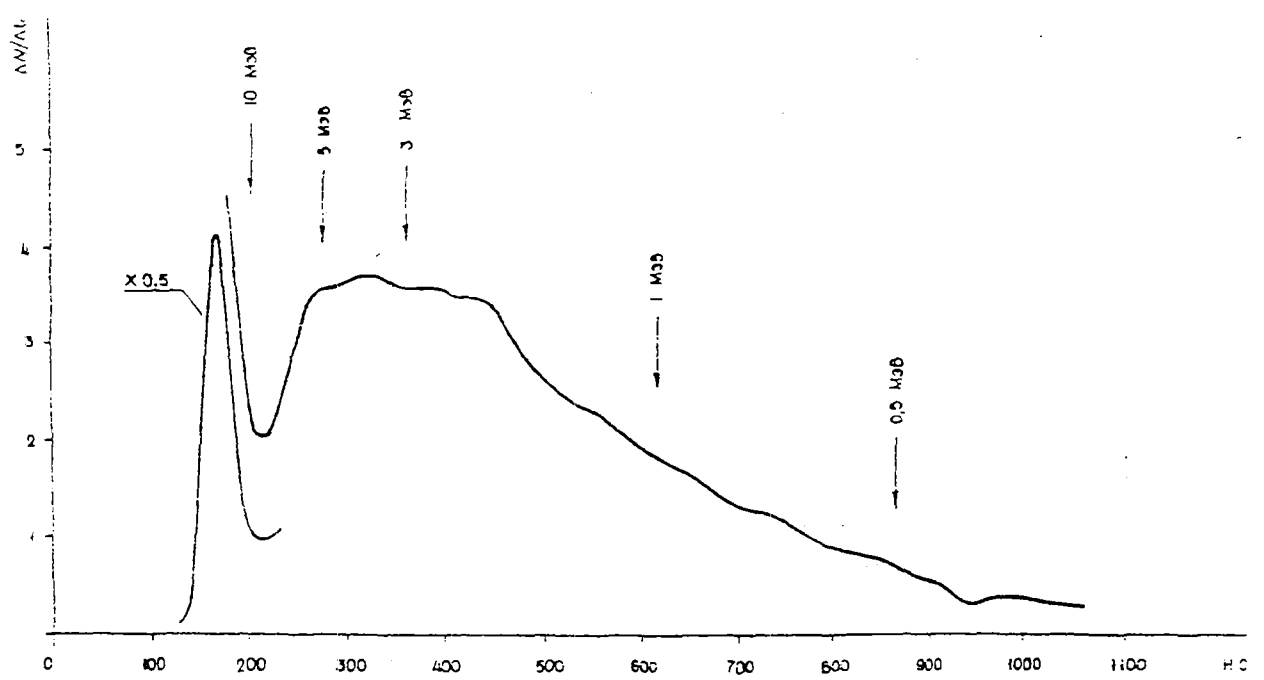

Fig. 4. Normalized instrumental spectrum from a hemispherical aluminium sample.

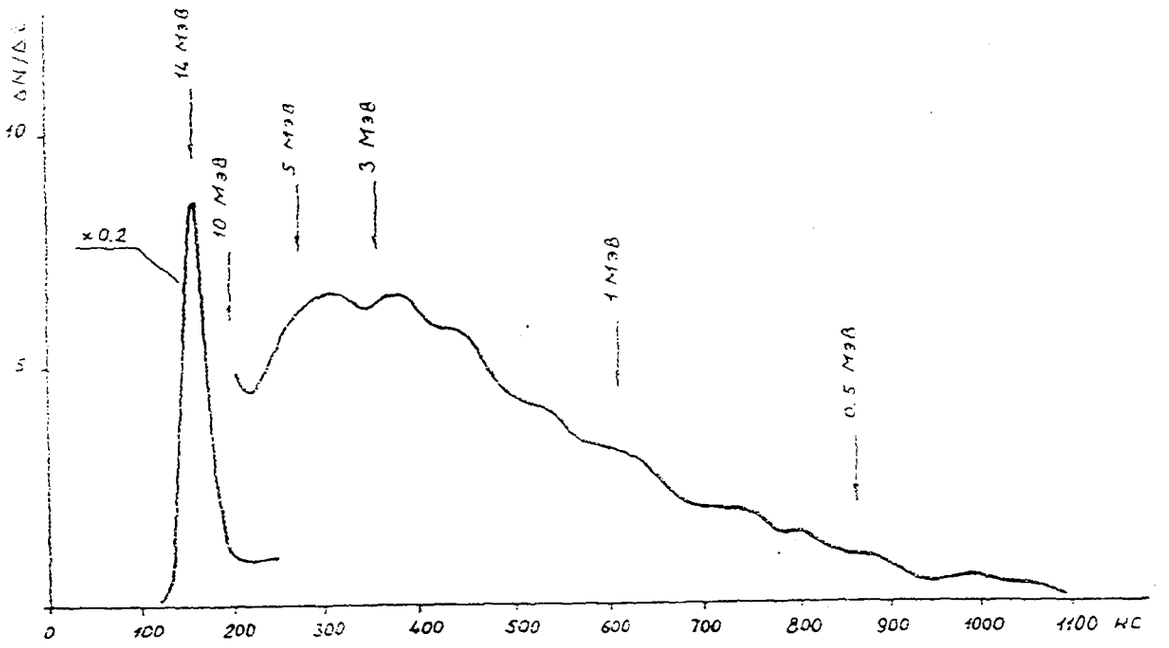

Fig. 5. Normalized instrumental spectrum from a spherical aluminium sample.

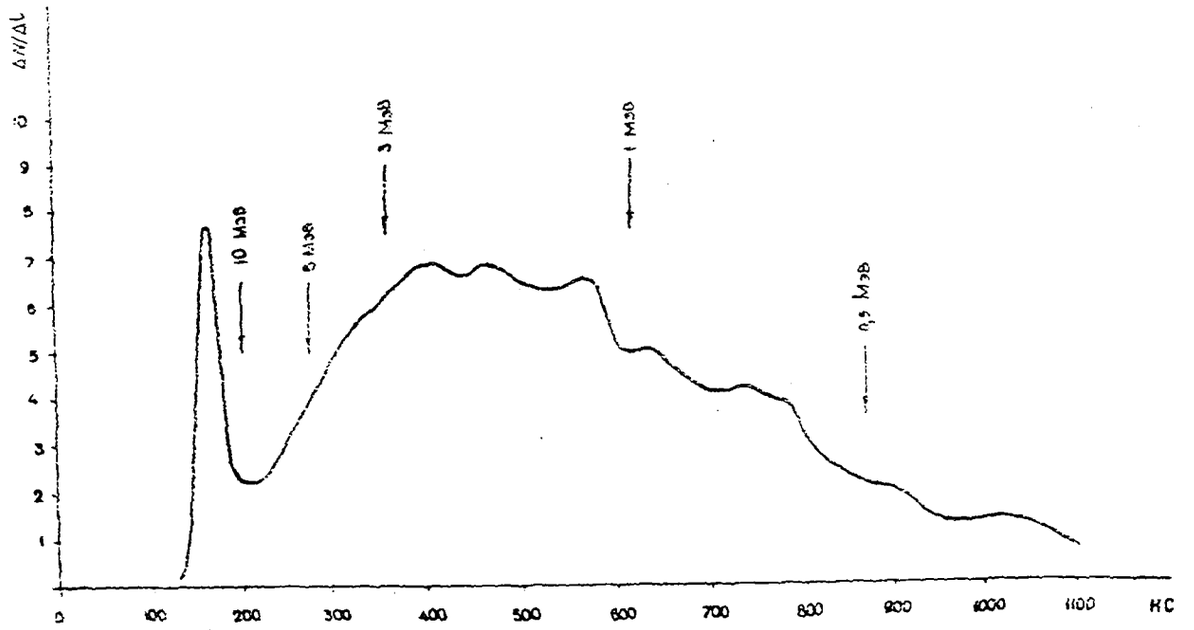

Fig. 6. Normalized instrumental spectrum from a hemispherical iron sample.

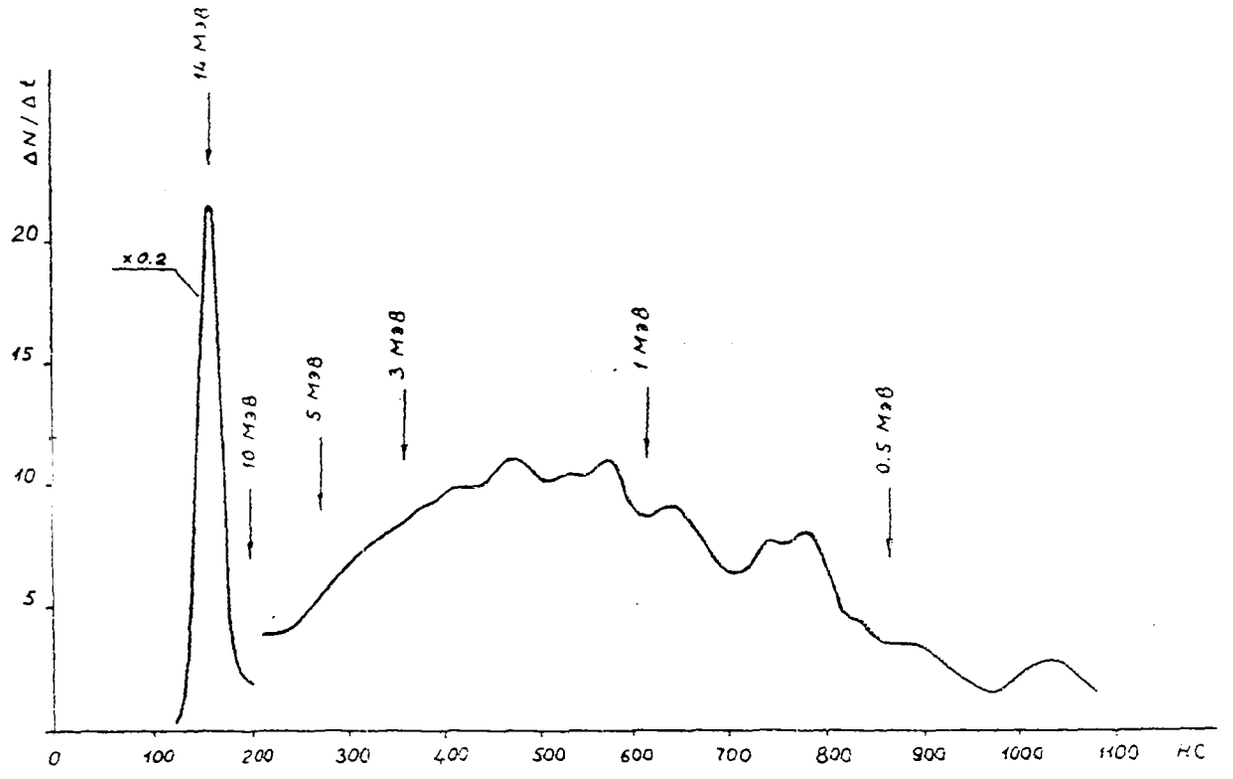

Fig. 7. Normalized instrumental spectrum from a spherical iron sample.

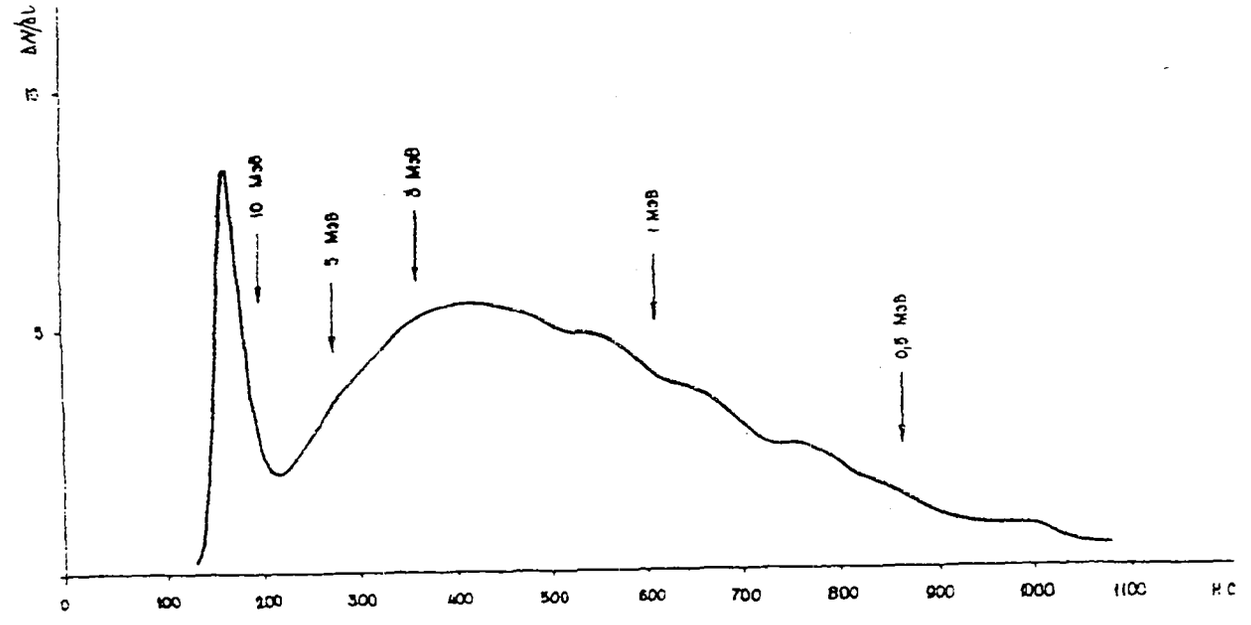

Fig. 8. Normalized instrumental spectrum from a hemispherical titanium sample.

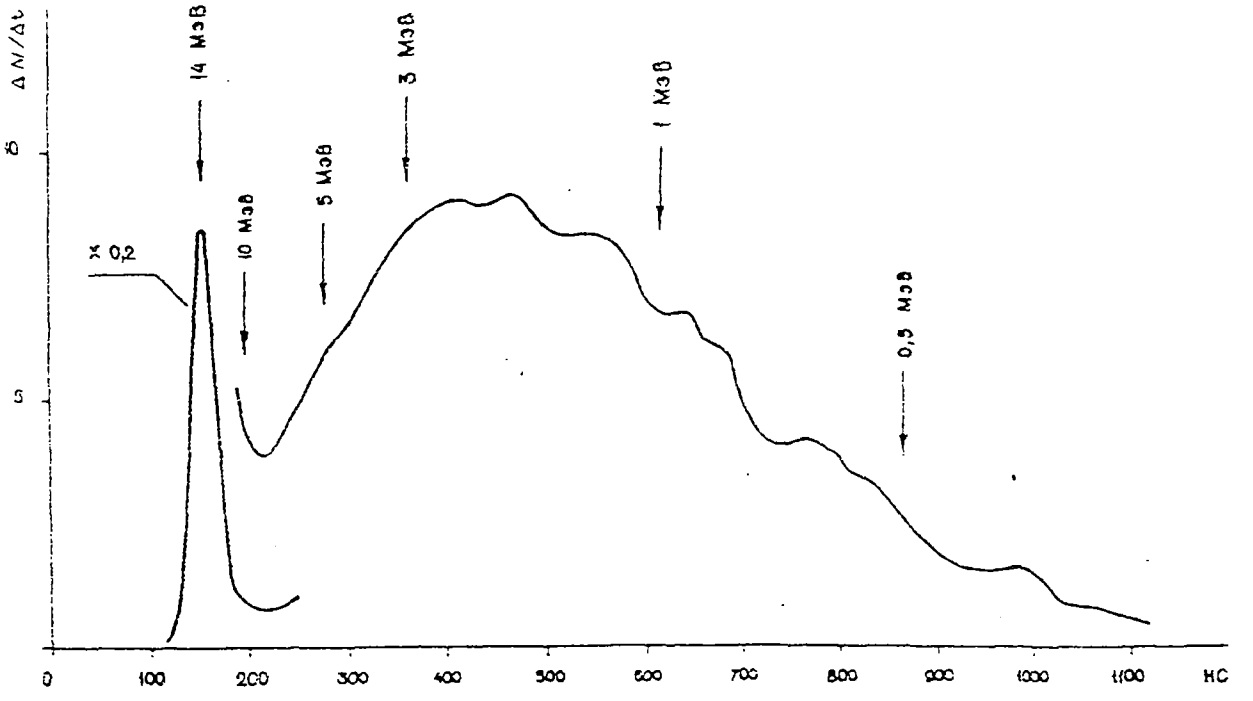

Fig. 9. Normalized instrumental spectrum from a spherical titanium sample.

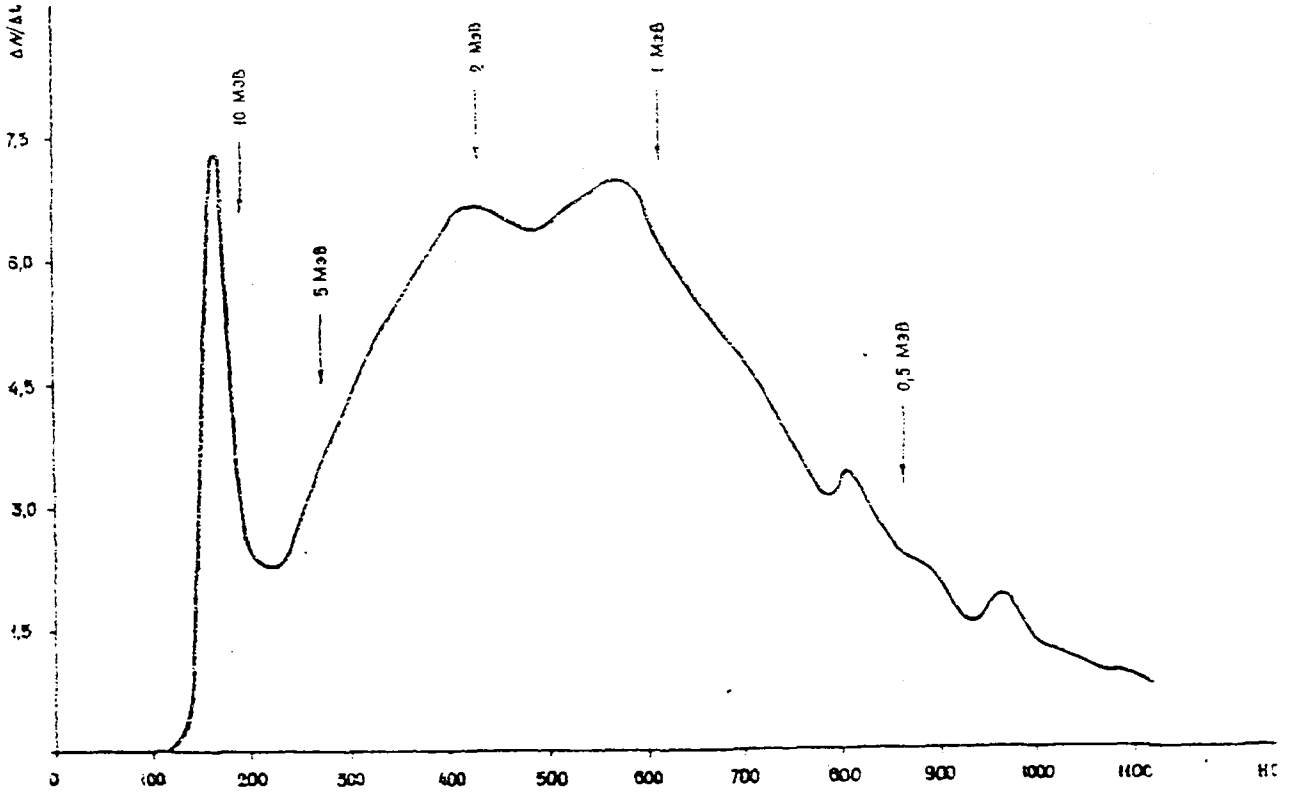

Fig. 10. Normalized instrumental spectrum from a hemispherical nickel sample.

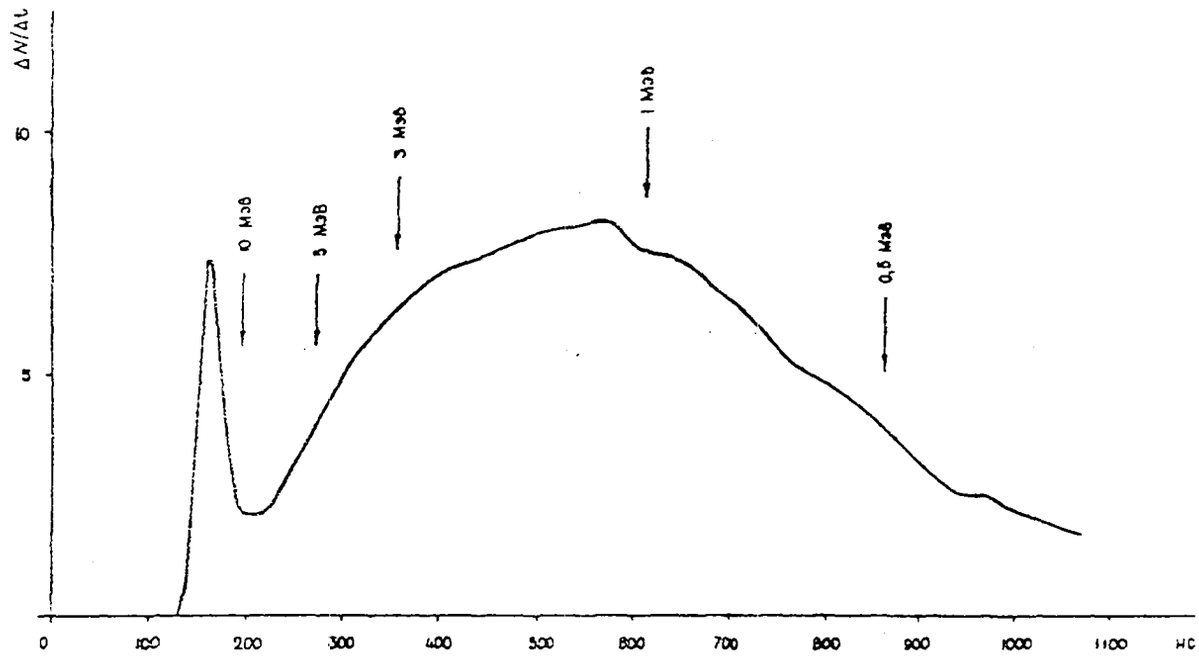

Fig. 11. Normalized instrumental spectrum from a spherical nickel sample.

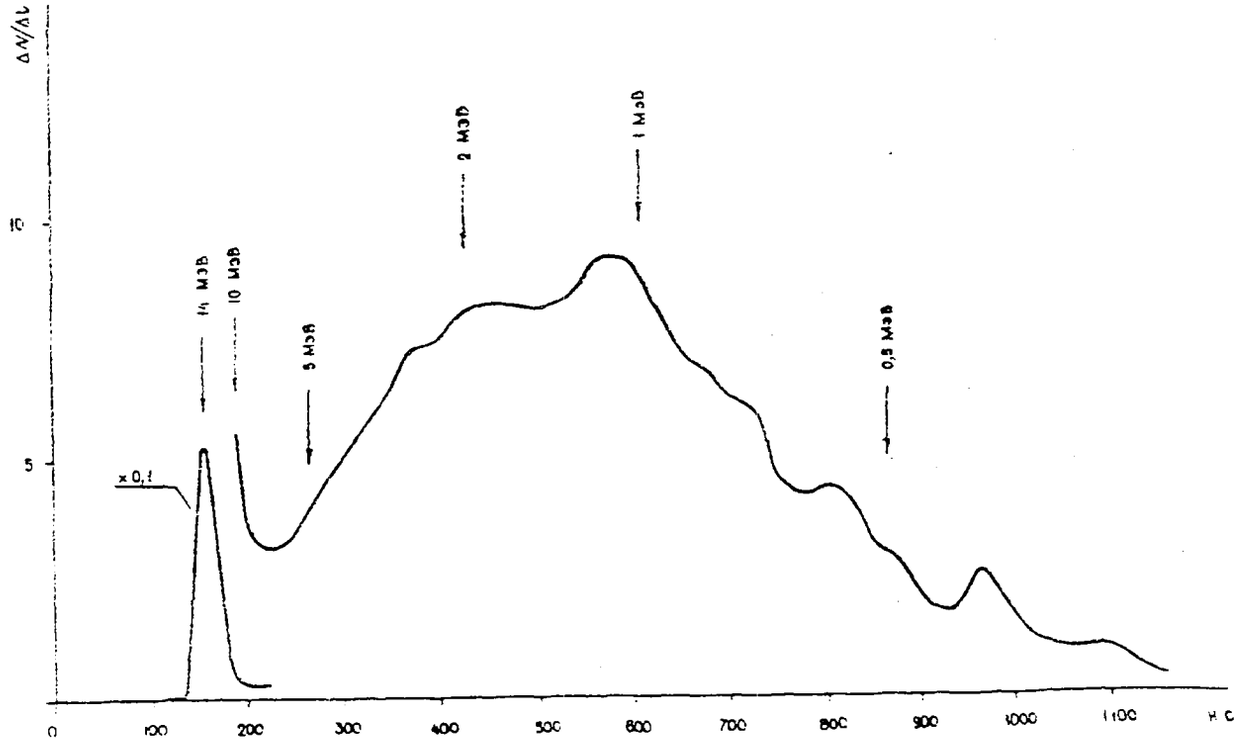

Fig. 12. Normalized instrumental spectrum from a hemispherical copper sample.

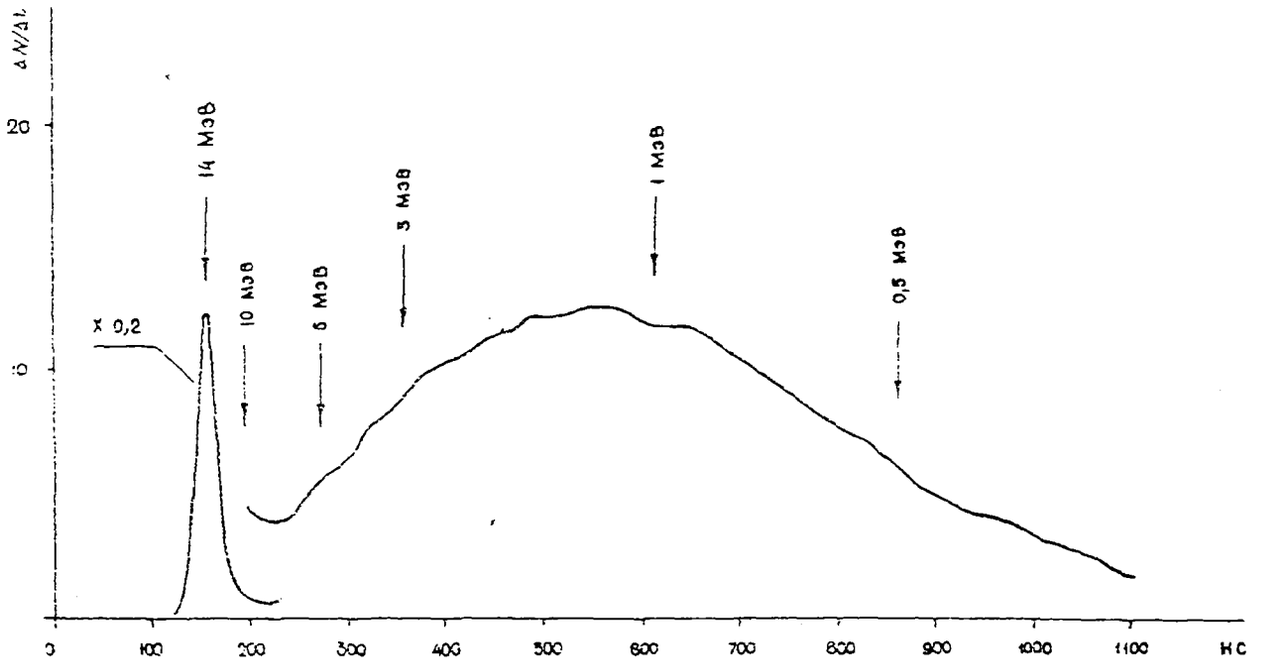

Fig. 13. Normalized instrumental spectrum from a spherical copper sample.

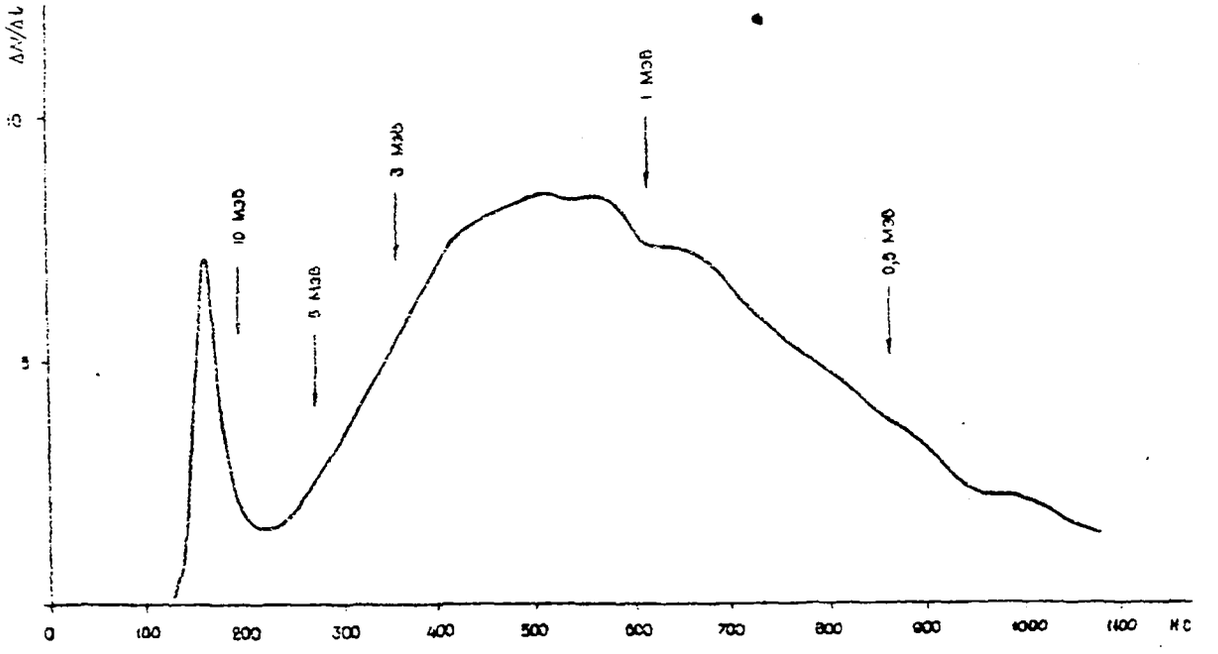

Fig. 14. Normalized instrumental spectrum from a hemispherical zirconium sample.

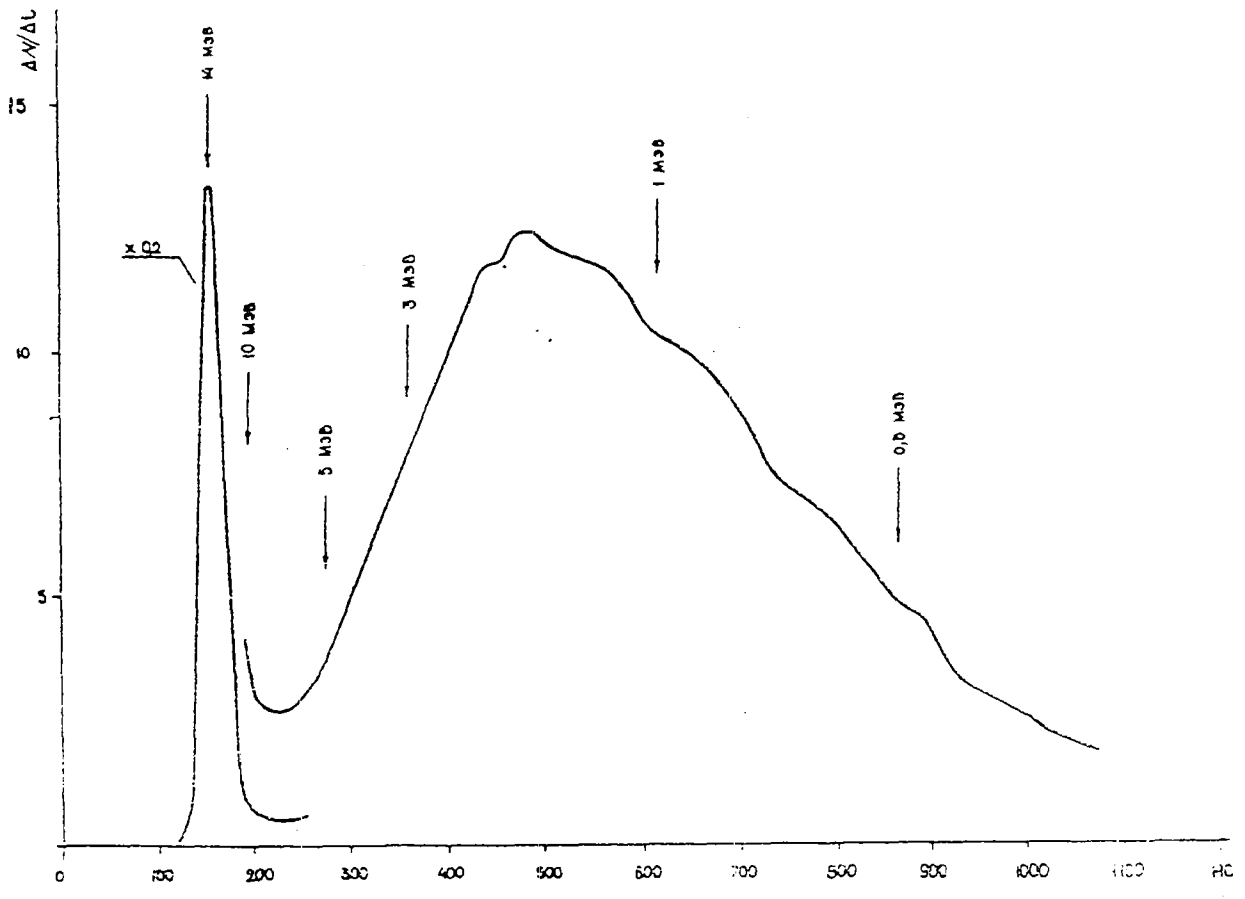

Fig. 15. Normalized instrumental spectrum from a spherical zirconium sample.

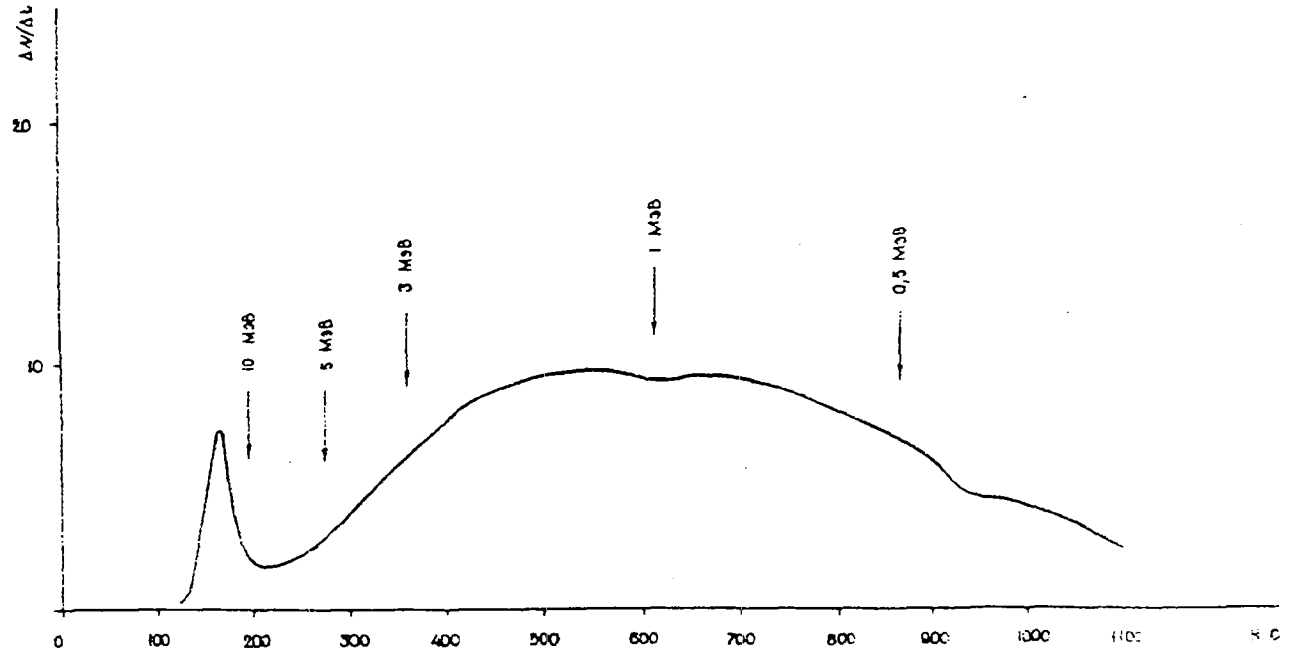

Fig. 16. Normalized instrumental spectrum from a hemispherical molybdenum sample.

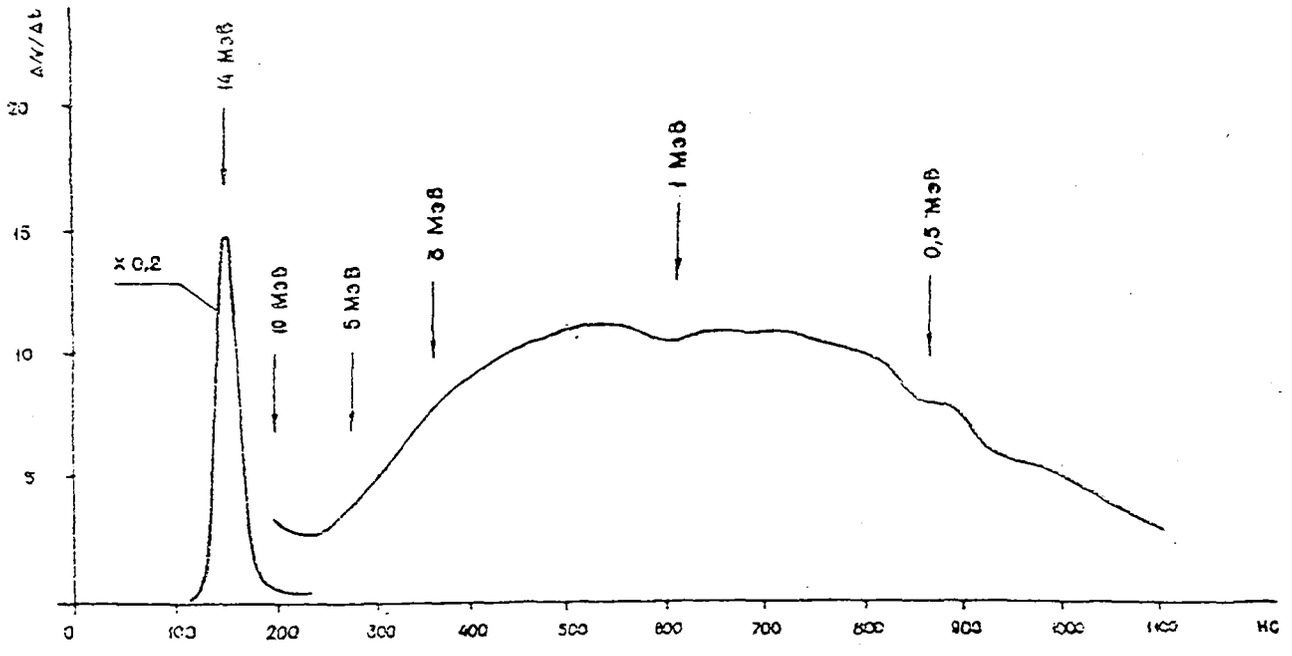

Fig. 17. Normalized instrumental spectrum from a spherical molybdenum sample.

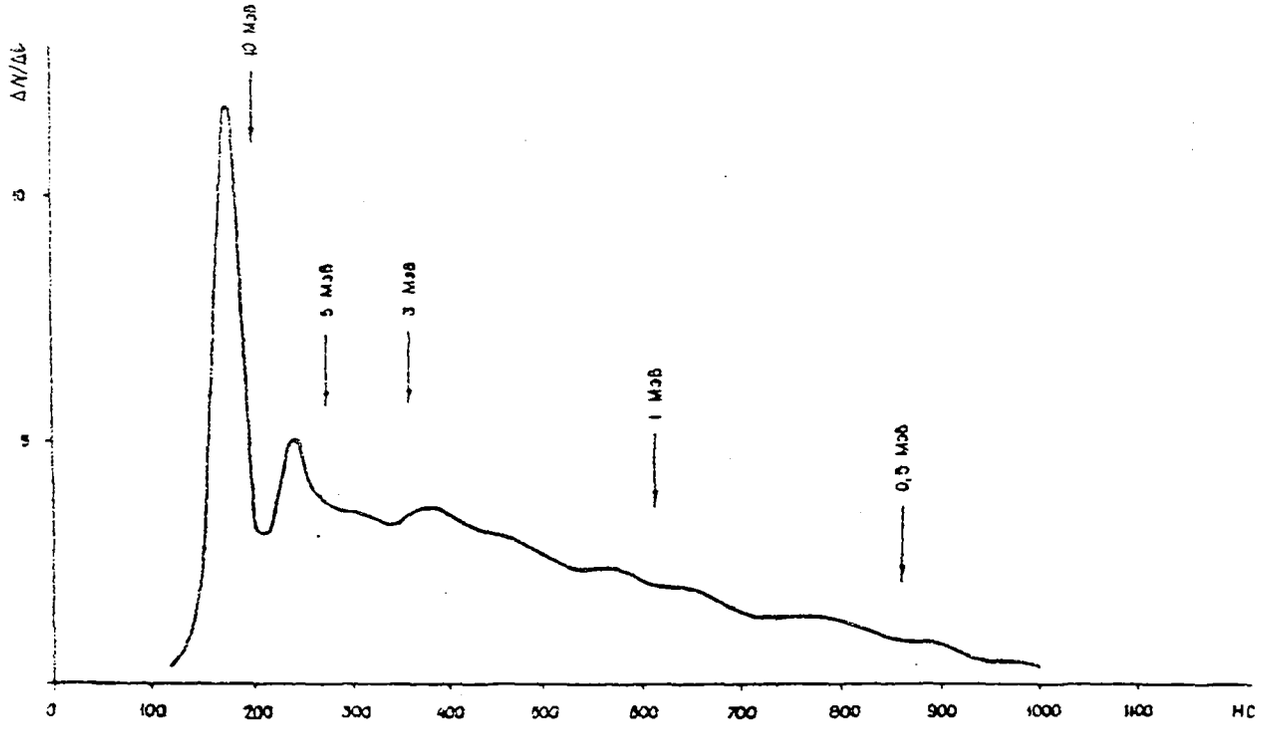

Fig. 18. Normalized instrumental spectrum from a hemispherical Teflon sample.

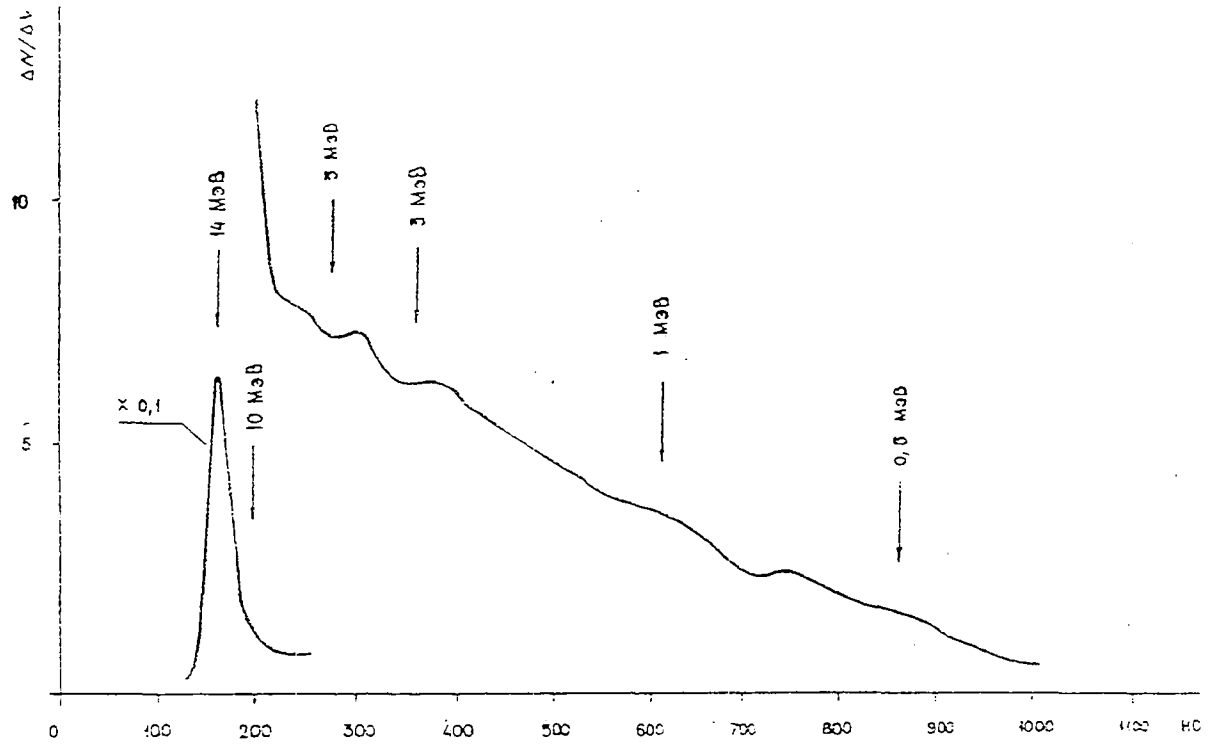

Fig. 19. Normalized instrumental spectrum from a spherical Teflon sample.

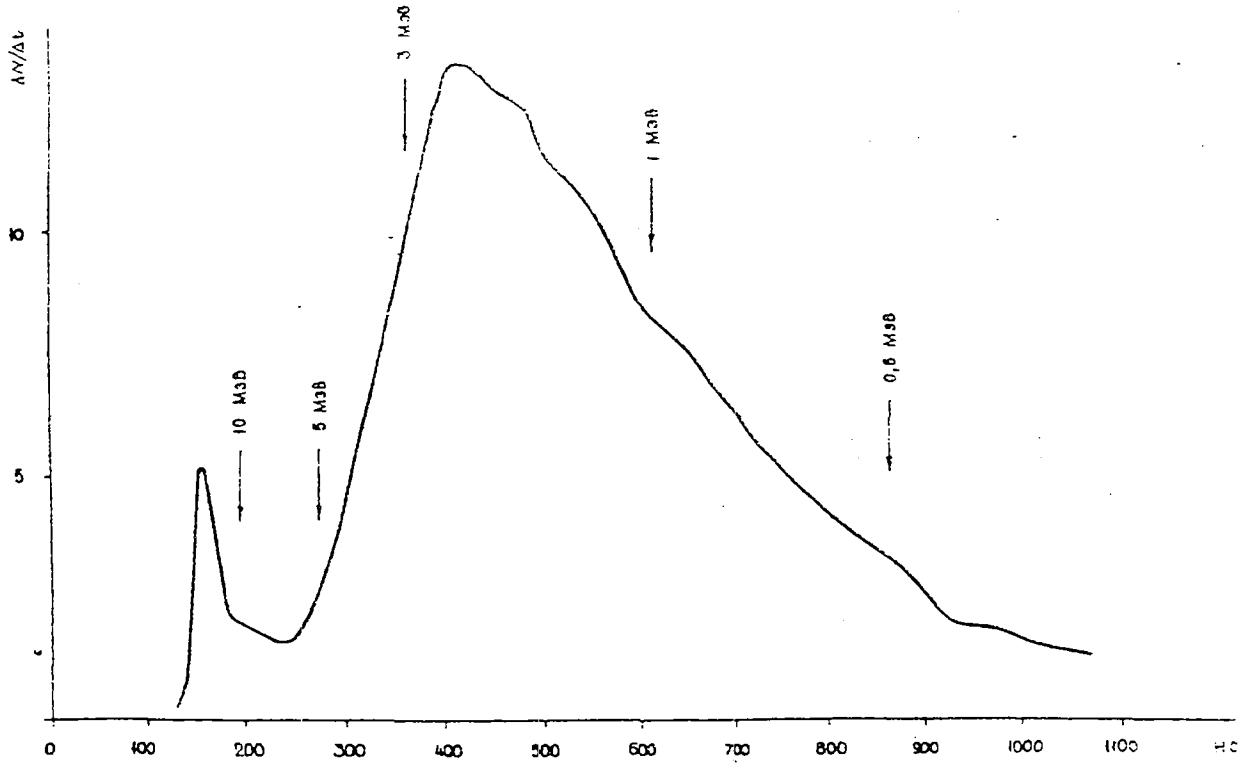

Fig. 20. Normalized instrumental spectrum from a hemispherical lead sample.

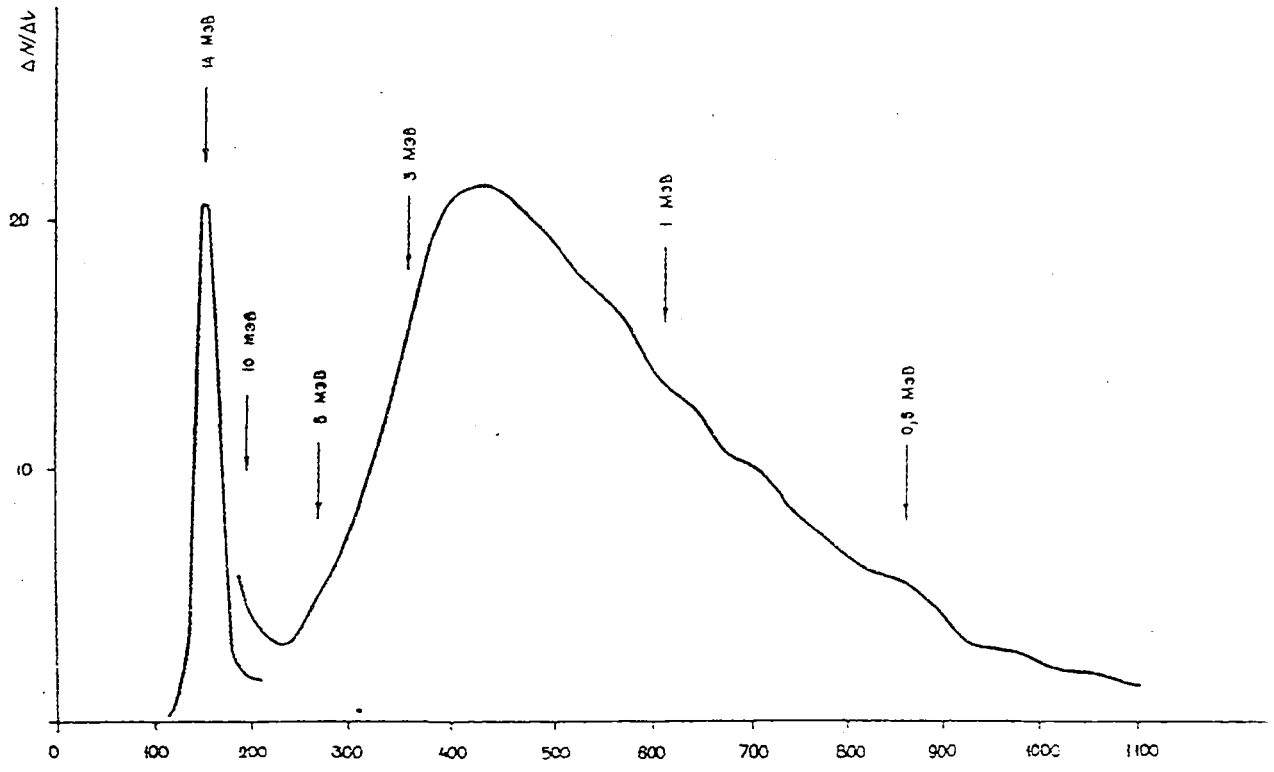

Fig. 21. Normalized instrumental spectrum from a spherical lead sample.

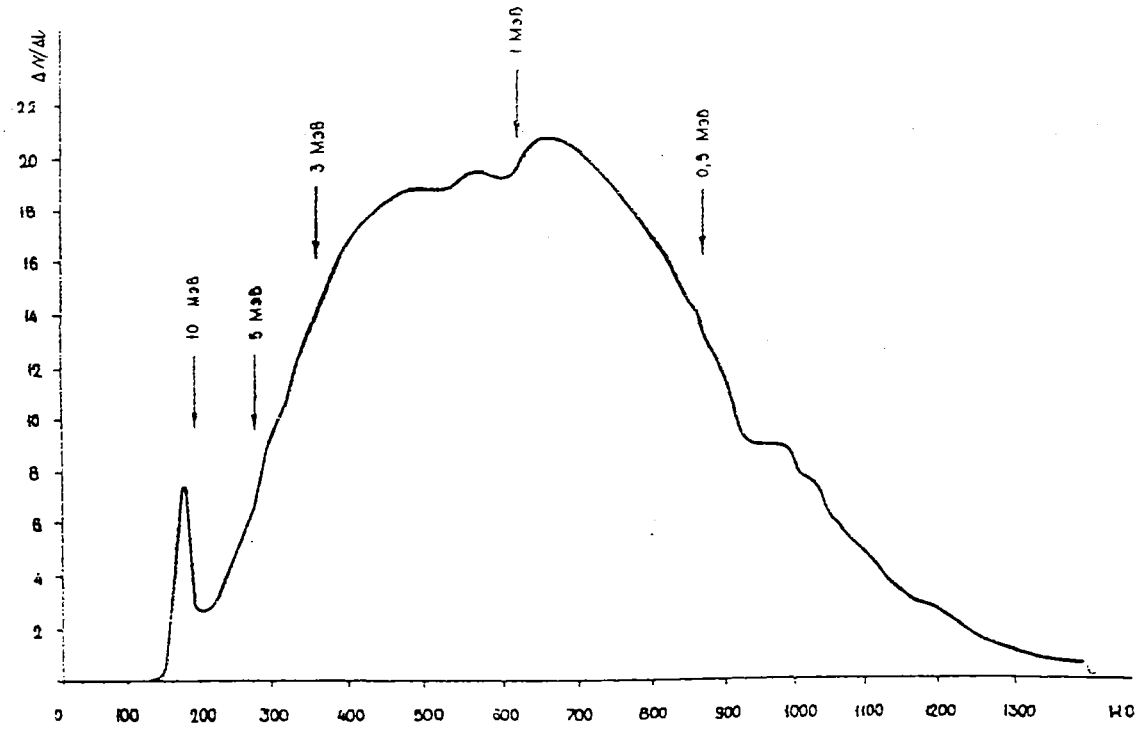

Fig. 22. Normalized instrumental spectrum from a hemispherical ^{238}U sample.

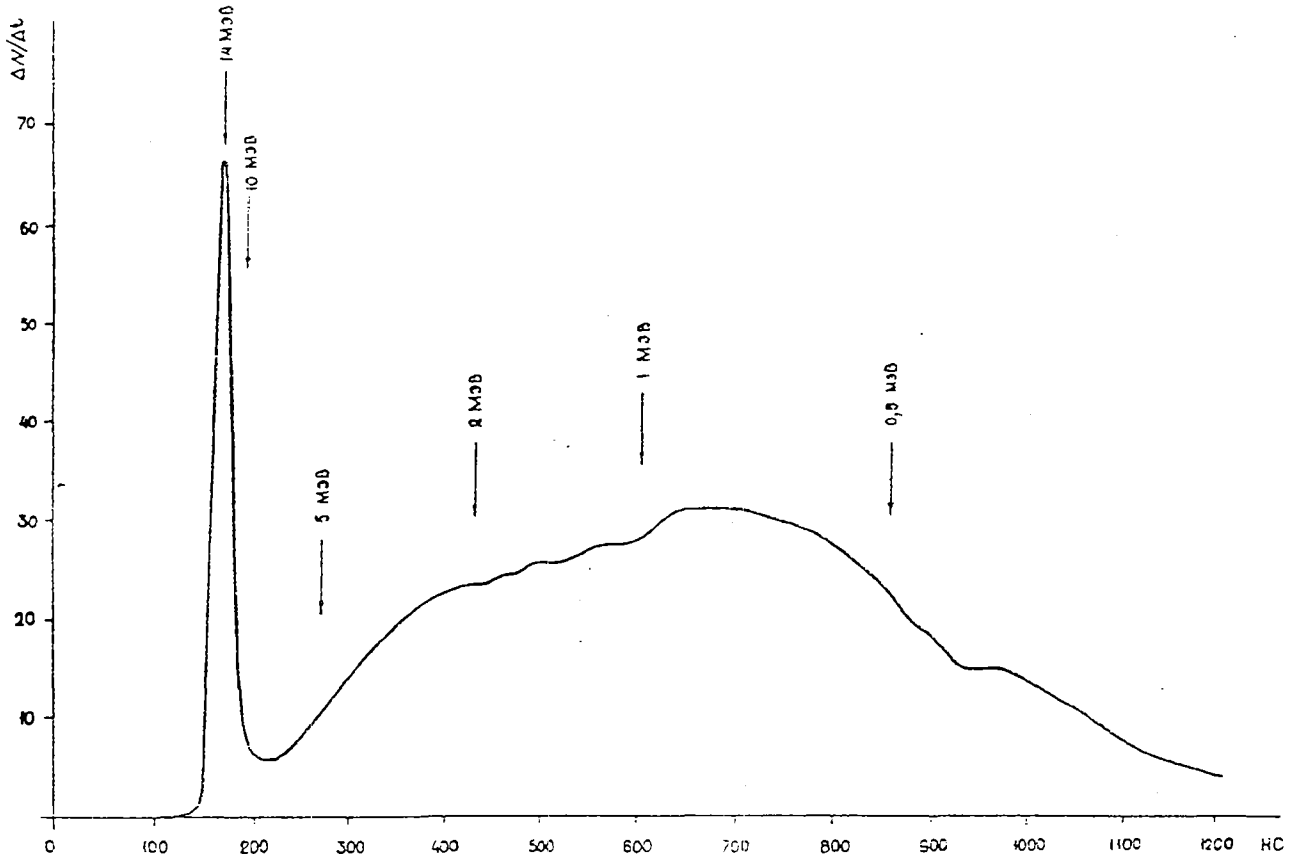

Fig. 23. Normalized instrumental spectrum from a spherical ^{238}U sample.

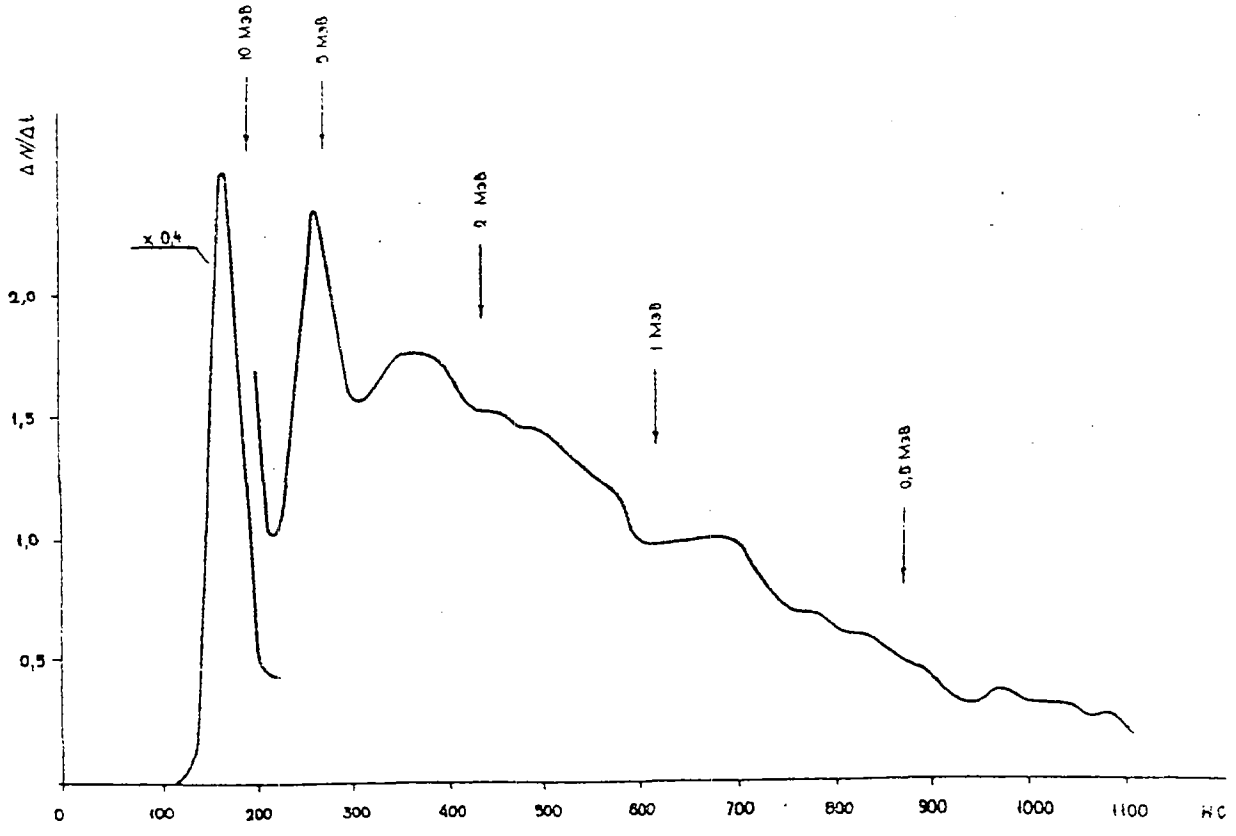

Fig. 24. Normalized instrumental spectrum from a hemispherical water sample.

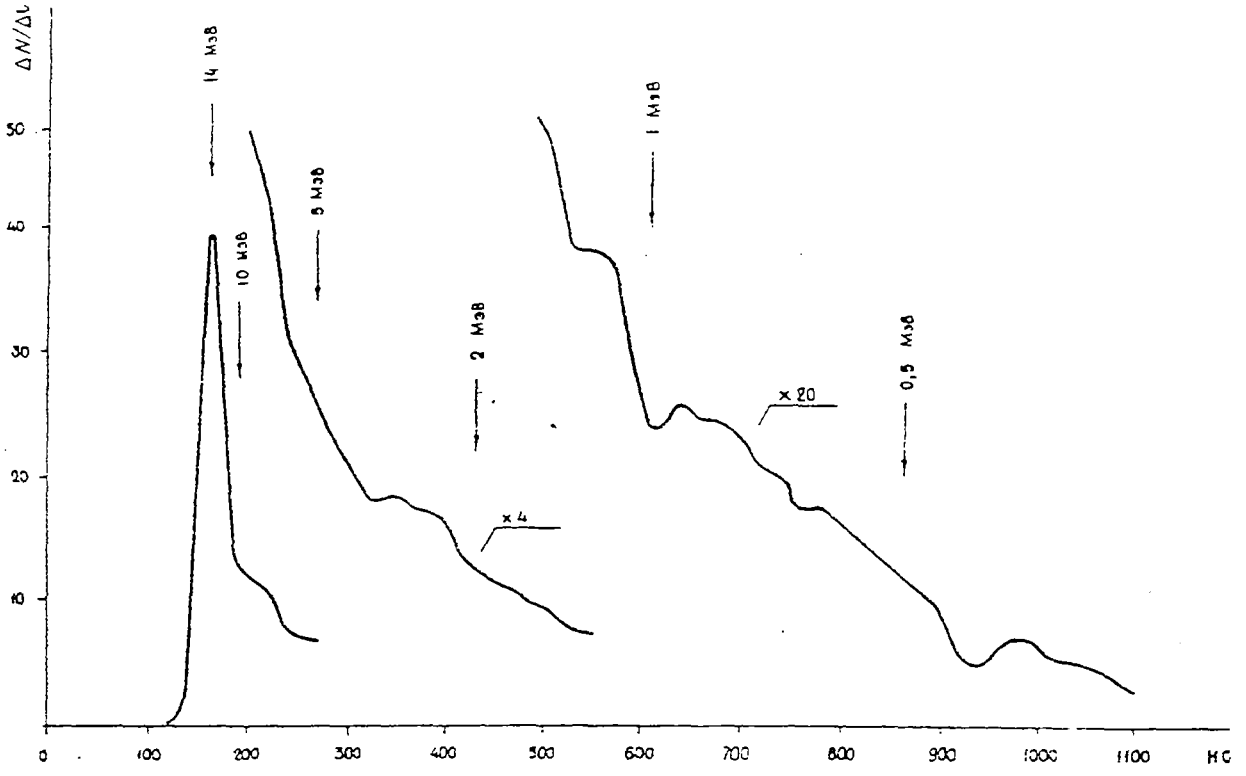

Fig. 25. Normalized instrumental spectrum from a spherical water sample.

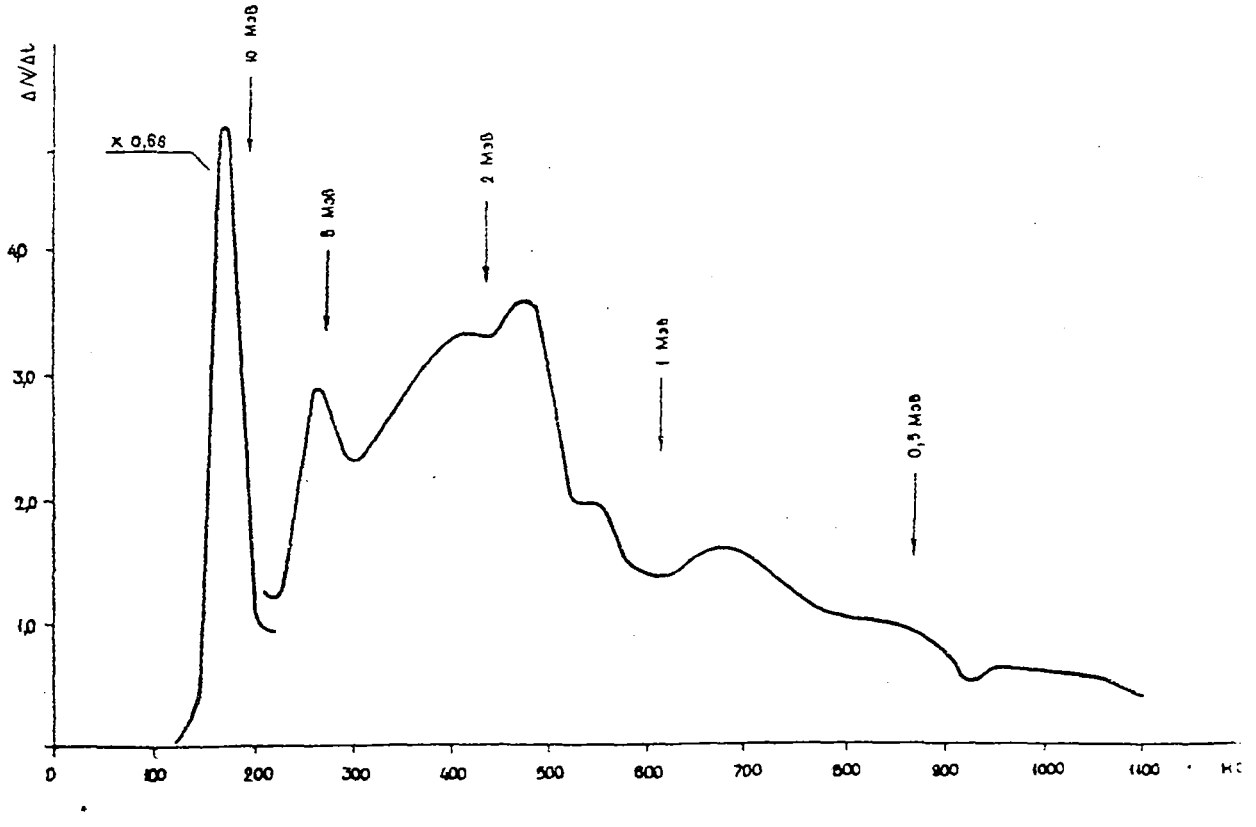

Fig. 26. Normalized instrumental spectrum from a hemispherical heavy water sample.

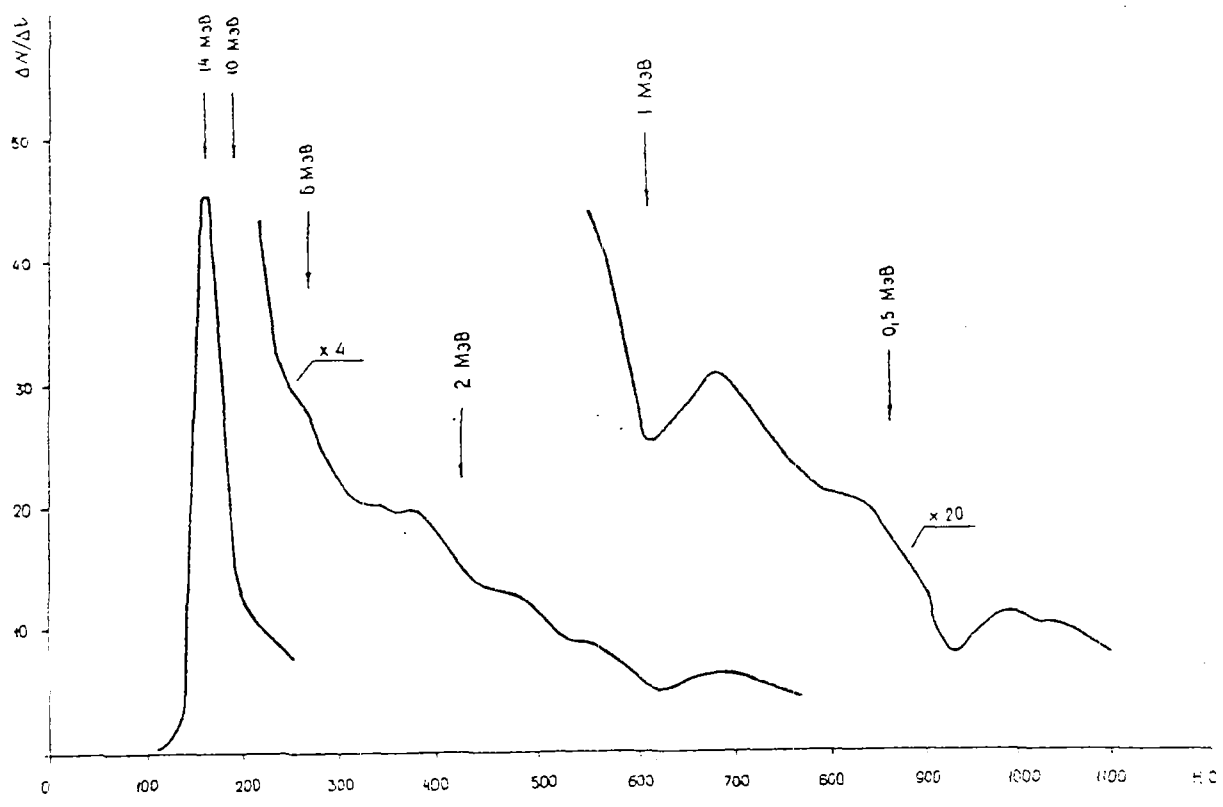

Fig. 27. Normalized instrumental spectrum from a spherical heavy water sample.

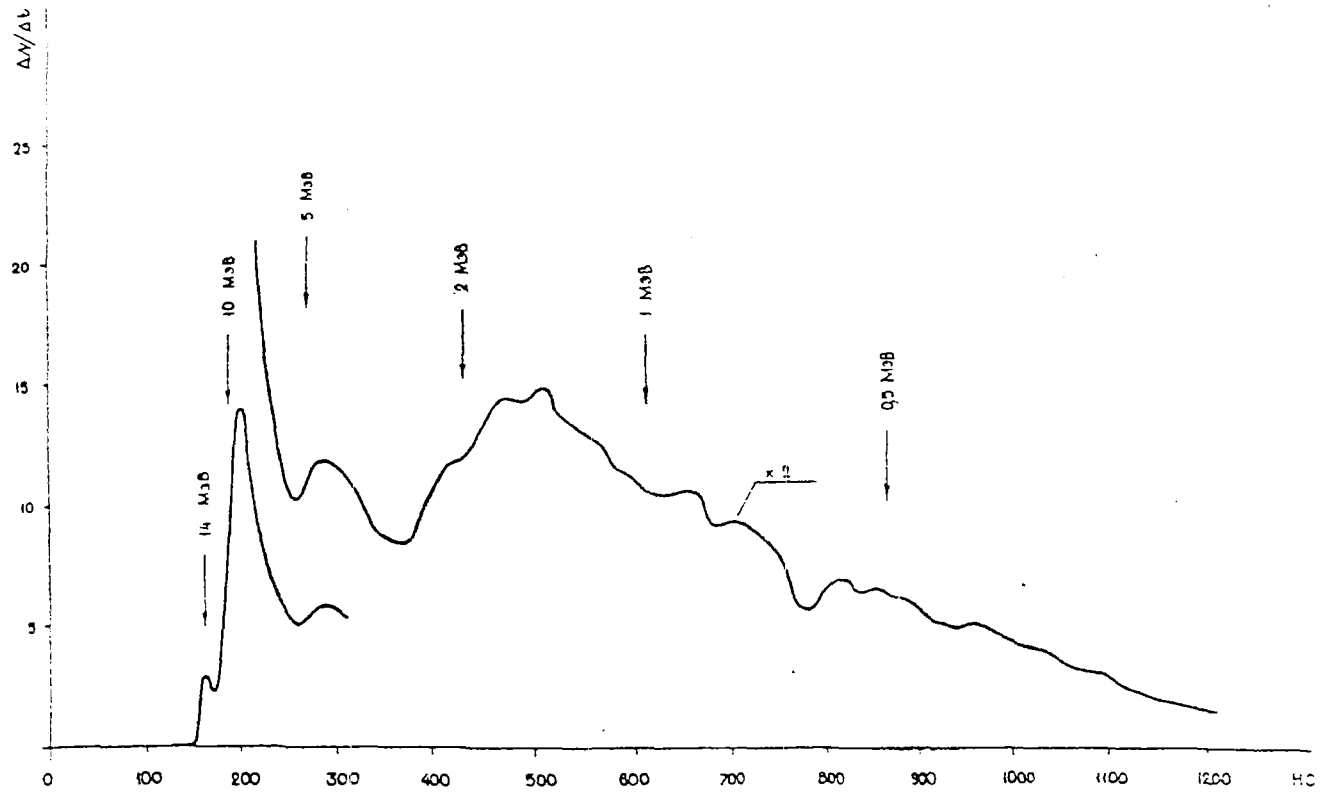

Fig. 28. Normalized instrumental spectrum from a hemispherical beryllium sample.

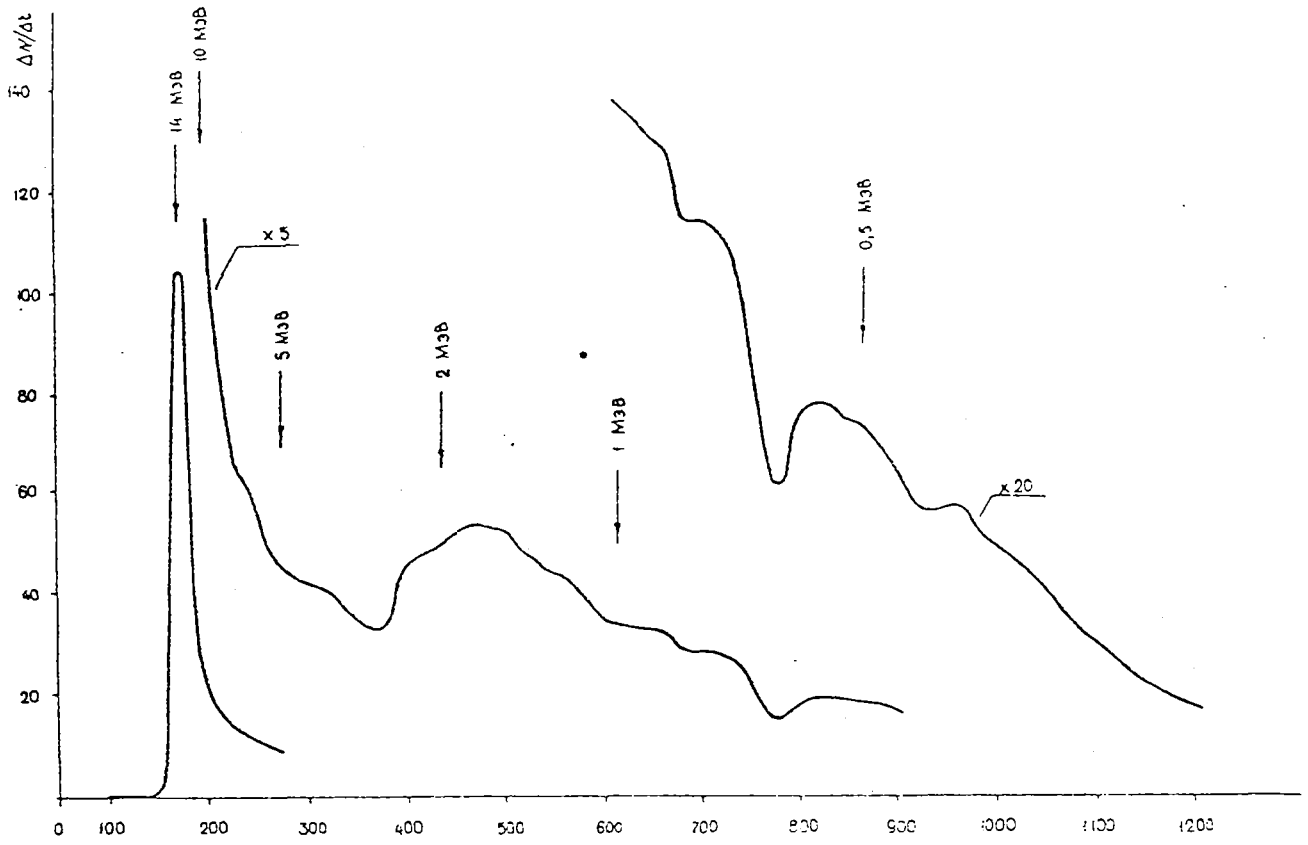

Fig. 29. Normalized instrumental spectrum from a spherical beryllium sample.

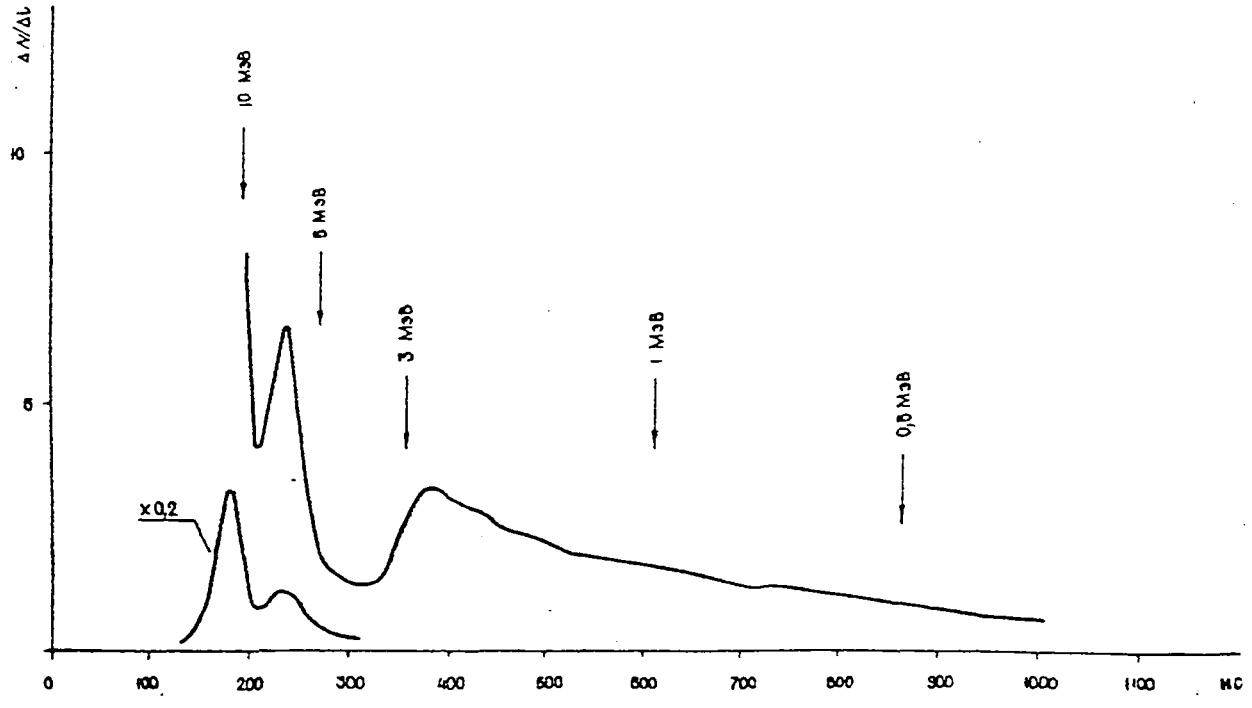

Fig. 30. Normalized instrumental spectrum from a hemispherical carbon sample.

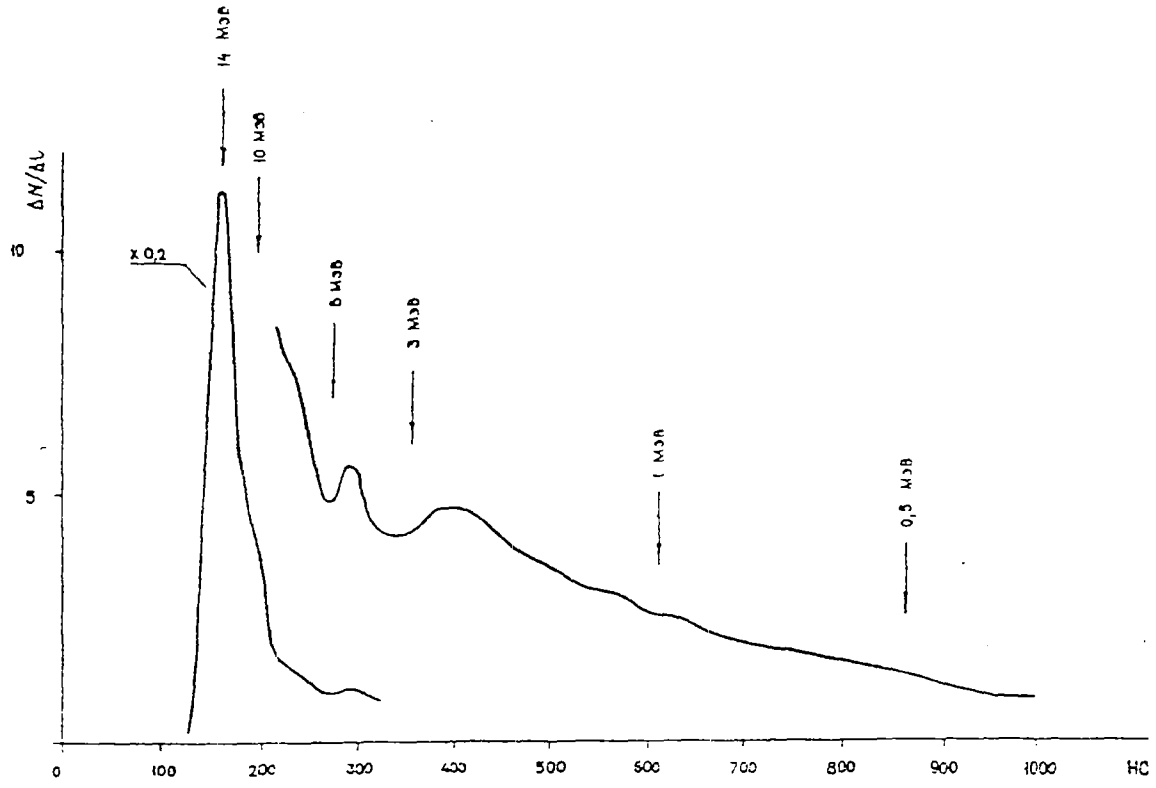

Fig. 31. Normalized instrumental spectrum from a spherical carbon sample.

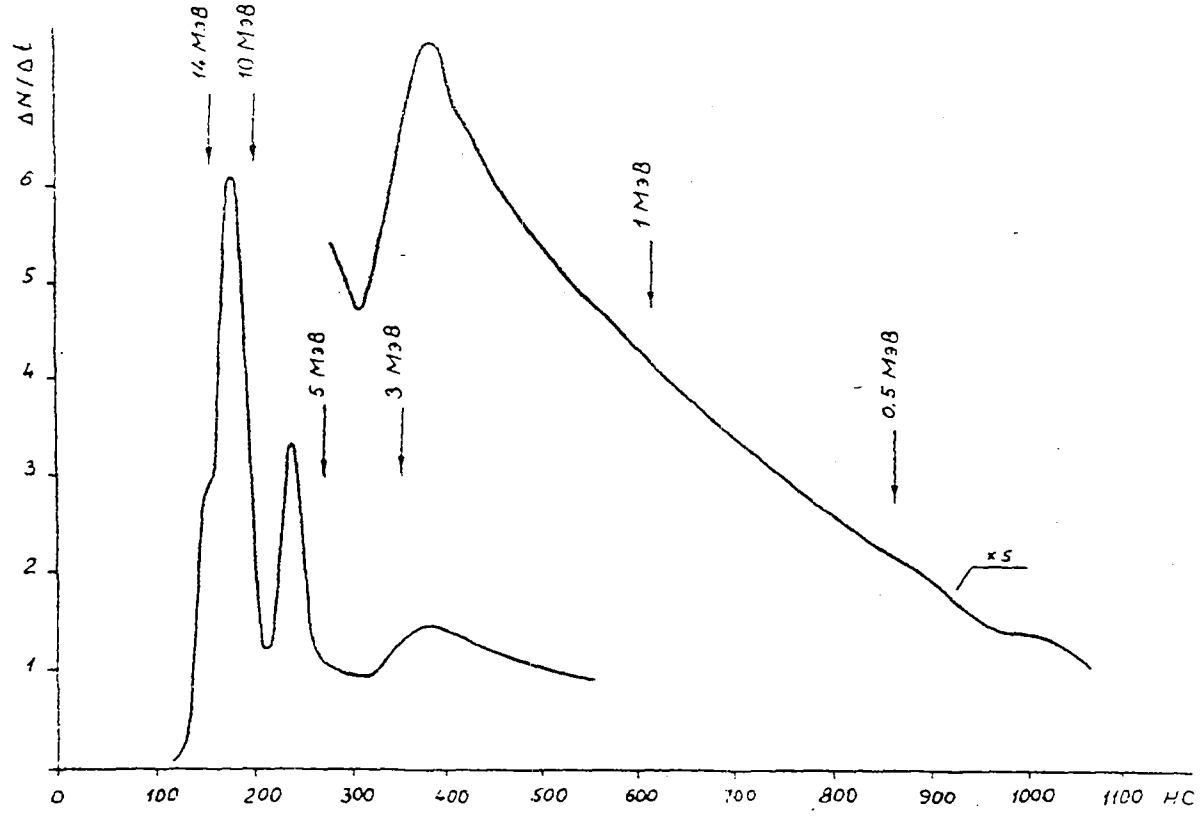

Fig. 32. Normalized instrumental spectrum from a hemispherical polyethylene sample.

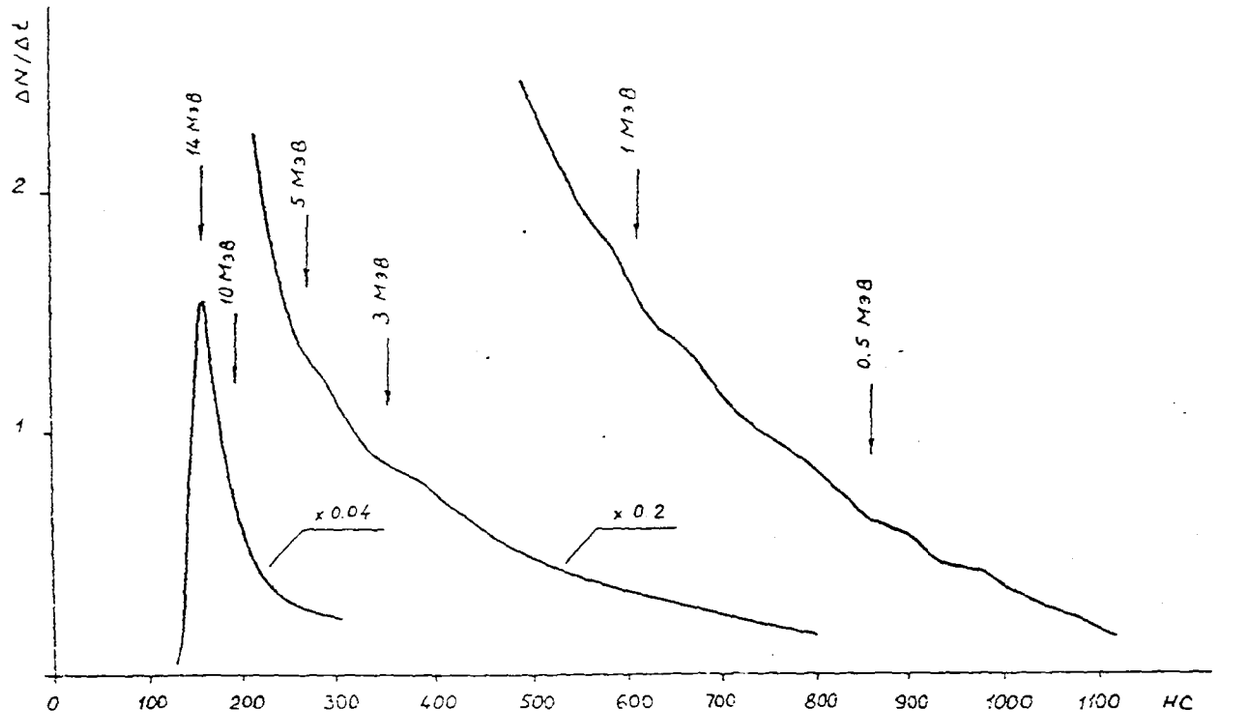

Fig. 33. Normalized instrumental spectrum from a spherical polyethylene sample.

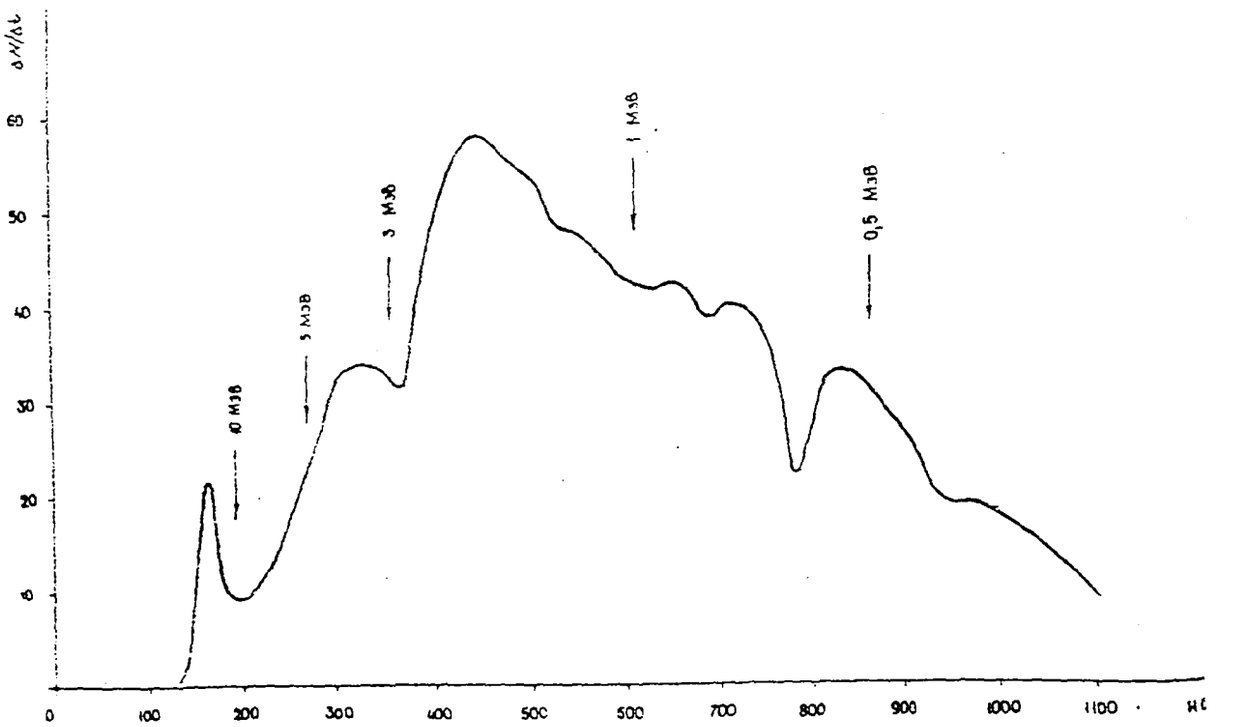

Fig. 34. Instrumental spectrum from a hemispherical ^{238}U sample through a 2 cm layer of beryllium.